Article

Cell

An Airway Protection Program Revealed by Sweeping Genetic Control of Vagal Afferents

Graphical Abstract

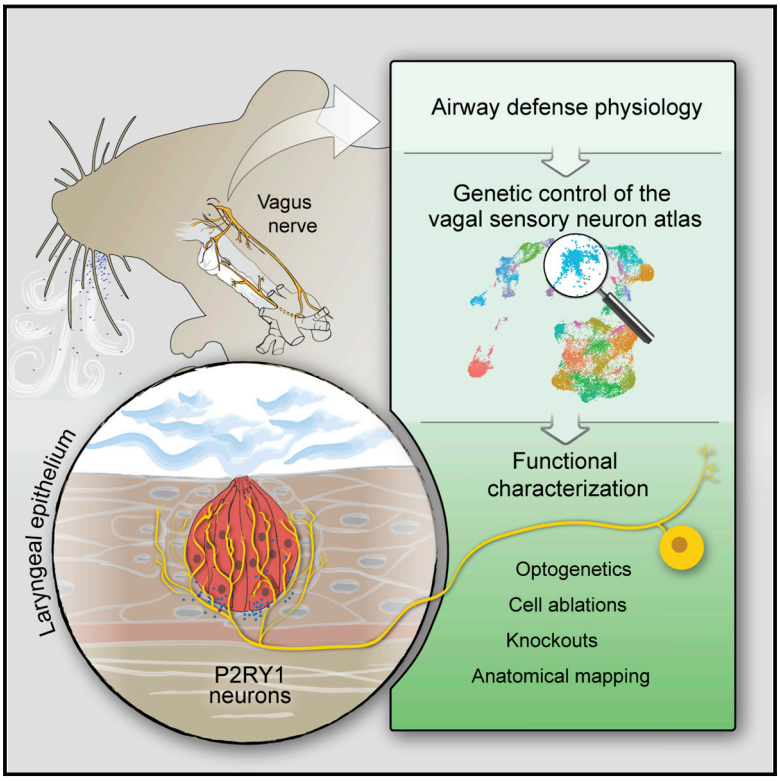

Highlights

- Broad genetic access enables functional dissection of a vagal sensory neuron atlas
- Rare P2RY1 sensory neurons guard the airways by engaging an airway defense program
- P2RY1 neurons innervate the laryngeal epithelium and appose laryngeal taste buds
- Epithelial cells detect laryngeal water/acid and communicate to P2RY1 neurons via ATP

Authors

Sara L. Prescott, Benjamin D. Umans, Erika K. Williams, Rachael D. Brust, Stephen D. Liberles

Correspondence

Stephen_Liberles@hms.harvard.edu

In Brief

Prescott and colleagues reveal a rare population of vagal sensory neurons that serve as a first-line defense in the upper airways to prevent infiltration and injury within the respiratory tract. The authors develop an expansive genetic toolkit that broadly covers a vagal/glossopharyngeal sensory neuron atlas and use genetic approaches to map, ablate, and control vagal sensory neuron populations, revealing sensory neurons that receive input from laryngeal epithelial cells through ATP and in response mediate critical aspects of airway defense.

Prescott et al., 2020, Cell *181*, 1–16
April 30, 2020
https://doi.org/10.1016/j.cell.2020.03.004

CellPress

Please cite this article in press as: Prescott et al., An Airway Protection Program Revealed by Sweeping Genetic Control of Vagal Afferents, Cell (2020), https://doi.org/10.1016/j.cell.2020.03.004

Article

Cell

An Airway Protection Program Revealed by Sweeping Genetic Control of Vagal Afferents

Sara L. Prescott,[1,2] Benjamin D. Umans,[1,2] Erika K. Williams,[1] Rachael D. Brust,[1] and Stephen D. Liberles[1,3,*]
[1]Howard Hughes Medical Institute, Department of Cell Biology, Harvard Medical School, Boston, MA 02115, USA
[2]These authors contributed equally
[3]Lead Contact
*Correspondence: Stephen_Liberles@hms.harvard.edu
https://doi.org/10.1016/j.cell.2020.03.004

SUMMARY

Sensory neurons initiate defensive reflexes that ensure airway integrity. Dysfunction of laryngeal neurons is life-threatening, causing pulmonary aspiration, dysphagia, and choking, yet relevant sensory pathways remain poorly understood. Here, we discover rare throat-innervating neurons (~100 neurons/mouse) that guard the airways against assault. We used genetic tools that broadly cover a vagal/glossopharyngeal sensory neuron atlas to map, ablate, and control specific afferent populations. Optogenetic activation of vagal P2RY1 neurons evokes a coordinated airway defense program—apnea, vocal fold adduction, swallowing, and expiratory reflexes. Ablation of vagal P2RY1 neurons eliminates protective responses to laryngeal water and acid challenge. Anatomical mapping revealed numerous laryngeal terminal types, with P2RY1 neurons forming corpuscular endings that appose laryngeal taste buds. Epithelial cells are primary airway sentinels that communicate with second-order P2RY1 neurons through ATP. These findings provide mechanistic insights into airway defense and a general molecular/genetic roadmap for internal organ sensation by the vagus nerve.

INTRODUCTION

The vagus nerve and other cranial nerves ensure the integrity of several major physiological systems. Peripheral sensory neurons monitor numerous vital parameters like blood pressure, airway volume, stomach distension, and circulating oxygen levels, and if potentially harmful deviations from equilibrium are detected, neural circuits are engaged to initiate corrective physiological and behavioral responses. Neuronal surveillance of internal organs is extensive but not comprehensively charted, with many neuronal safeguards likely remaining so far hidden. Moreover, dysfunction of organ-to-brain communication can be lethal. One of the most fundamental functions of the vagus nerve is to provide the first line of defense that protects the airways from injury. Defects in vagally mediated reflexes in the upper airways cause some of the most pervasive and severe clinical problems associated with aging including dysphagia (difficulty swallowing), weight loss, choking, speech impairment, and respiratory tract infections such as aspiration pneumonia (Jadcherla et al., 2010; Ludlow, 2015; Santoso et al., 2019). Furthermore, hyperactivity or sensitization of upper airway neurons may contribute to asthma, chronic cough, and sudden infant death syndrome (SIDS). Here, we used information and genetic tools resulting from a comprehensive survey of vagal sensory neuron diversity to gain insights into physiological mechanisms underlying airway defense.

The larynx, as gateway to the respiratory system, is a hotspot for neuronal innervation (Ludlow, 2015; Steele and Miller, 2010). The larynx adjoins the digestive tract, and ingested food and water, as well as expelled stomach contents, must transit over the larynx without penetrating the airways. A complex network of laryngeal neurons guards the airways against infiltration by evoking characteristic occlusion and expulsion reflexes (Coleridge et al., 1989; Ludlow, 2015; Mazzone and Undem, 2016; Steele and Miller, 2010). For example, each swallow evokes reflexive responses that include (1) stopping inspiration to prevent pulmonary aspiration, (2) vocal fold adduction, and (3) laryngeal vestibule closure through hyoid bone elevation and epiglottis descent. If foreign material does enter the airways, secondary clearance reflexes are evoked, including cough (in some species), gag, expiratory reflexes, and pharyngeal swallow.

The upper airways are densely innervated by the vagus nerve through the superior laryngeal (SLN) and recurrent laryngeal (RLN) nerve branches (Figure 1A) (Coleridge et al., 1989; Ludlow, 2015; Mazzone and Undem, 2016; Steele and Miller, 2010). The internal branch of the SLN provides the major sensory innervation of the larynx, from the vocal folds to the epiglottis, as well as the caudal pharynx. RLN afferents instead predominate below the vocal folds, with dense innervation of the trachea and lung. Loss of SLN function by nerve injury or transient application of local anesthetic causes dysphagia, incomplete laryngeal closure, and risk of airway aspiration (Jadcherla et al., 2010; Jafari et al., 2003; Santoso et al., 2019). Electrically stimulating the SLN evokes hallmarks of airway protection including cough, apnea (breathing pause), vocal fold adduction, and fictive swallowing (Bolser, 1991; Doty, 1951). These studies highlighted the general importance of neuronal feedback for airway protection, but did not distinguish the contributions of various vagal neuron subtypes or the molecular mechanisms they employ.

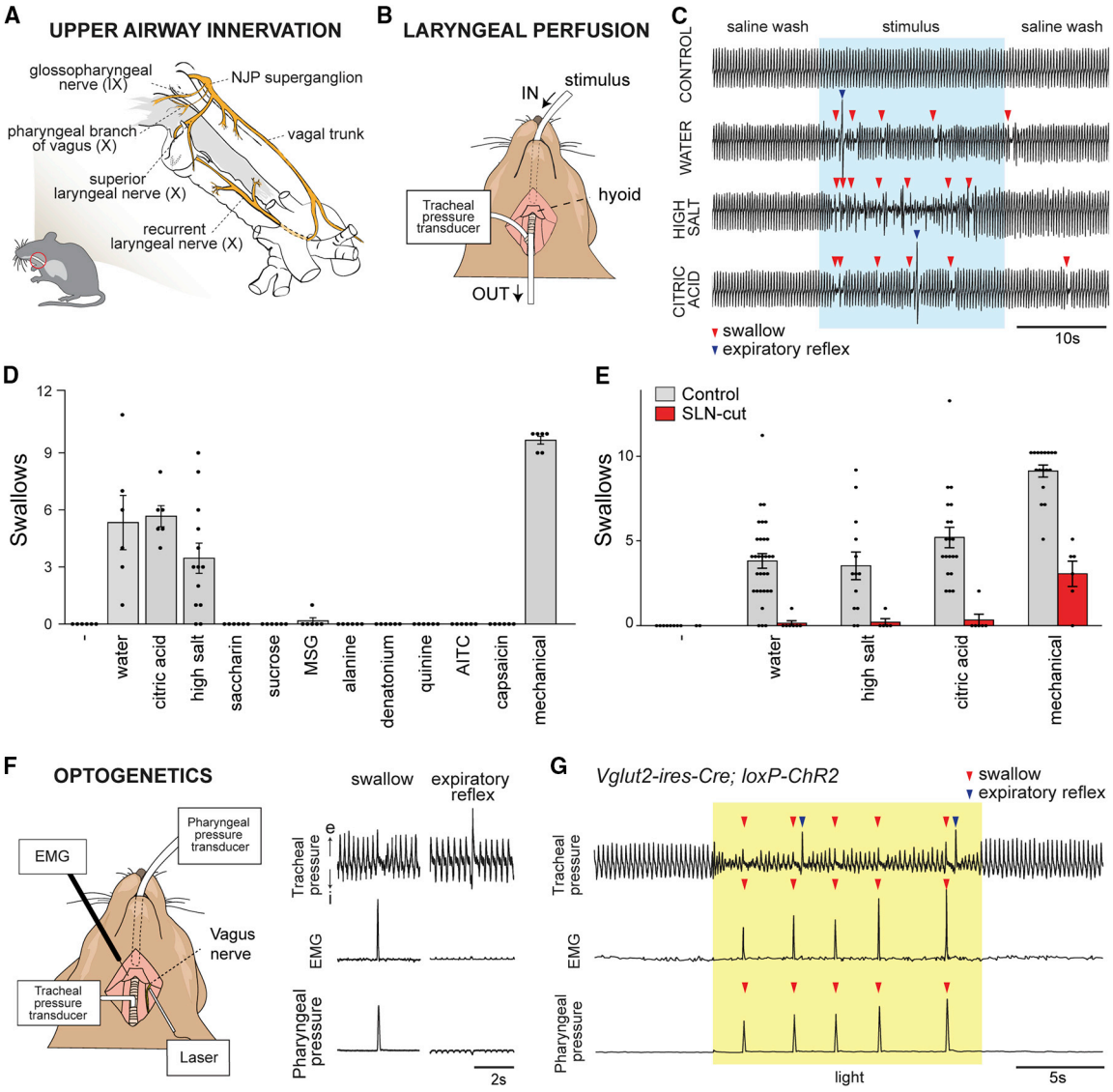

Figure 1. Evoking Swallows and Expiratory Reflexes with Laryngeal Stimulation and Light

(A) Cartoon of upper airway innervation.

(B) Schematic for perfusion of laryngeal stimuli.

(C) Representative respiratory rhythms during (blue shading) delivery of isotonic saline (control), water, high salt (1,500 mOsm), and citric acid (25 mM) with swallows (red triangles) and expiratory reflexes (blue triangles) noted.

(D) Swallows (n = 6–13 mice, mean ± SEM) were counted during laryngeal application of stimuli (see STAR Methods).

(E) Swallows were counted before (control, gray) or after (SLN-cut, red) acute bilateral SLN transection (n = 2–31 mice, mean ± SEM).

(F) Cartoon (left) depicting optogenetics paradigm under urethane, and (right) changes in tracheal pressure (i, inspiration; e, expiration), digastric muscle electromyography (EMG), and pharyngeal pressure during a representative swallow and expiratory reflex.

(G) Optogenetic stimulation (vagal trunk) in *Vglut2-ires-Cre; loxP-Chr2* mice resulted in swallows (red triangles) and expiratory reflexes (blue triangles). Representative traces of tracheal pressure, digastric muscle EMG, and pharyngeal pressure over time are shown, yellow shading: light stimulation (20 Hz).

Airway threats are detected throughout the larynx, with complex neuronal arbors found on the epiglottis and vocal folds, and in the postcricoid and arytenoid regions (Feindel, 1956; Mu and Sanders, 2000; Travers and Nicklas, 1990; Yamamoto et al., 1997). A multitude of laryngeal sensory terminals have been described, including submucosal and epithelial free endings, ivy-like laminar (hederiform) endings, corpuscular endings, cough receptors, and endings near taste buds. The functions of particular terminal morphologies have been debated, with models based largely on the proximity of terminals to mechanosensory or chemosensory hotspots. However, different terminal types typically display overlapping regions of innervation in the larynx, and consistent anatomical nomenclature is lacking. As a result, previous descriptors may redundantly refer to the

same terminal type, or incorrectly group together sensory neurons with different response profiles. We reasoned that genetic tools might provide more consistency across studies and also allow for specific functional manipulation to resolve the sensory roles of different laryngeal terminals.

Nerve recordings revealed that laryngeal sensory neurons detect various mechanical and chemical stimuli (Harding et al., 1978; Sampson and Eyzaguirre, 1964; Sant'Ambrogio et al., 1991; Smith and Hanamori, 1991; Storey, 1968), including (1) water, salt, and pharyngeal/laryngeal force from ingested food and drink, (2) acid, bile, and esophageal force from regurgitated stomach contents, and (3) invasive threats, such as pathogens and irritants like smoke, oxidants, and dust particles. Various mechanisms have been proposed for irritant and pathogen detection (Baral et al., 2018; Bessac and Jordt, 2008; Canning et al., 2004; Han et al., 2018; Krasteva et al., 2011; Tizzano et al., 2010), but less is understood about the diversity and organization of sensory pathways that protect the airways from penetration by food, drink, and gastric reflux. Water, salt, acid, and force stimulate the SLN (Smith and Hanamori, 1991) and also evoke defensive reflexes including apnea, vocal fold adduction, pharyngeal swallow, and cough (Canning et al., 2004; Kovar et al., 1979; Shingai et al., 1989). Water responses are particularly robust in the larynx, yet primary sensory cells are unknown. It is unclear whether water-sensing and acid-sensing laryngeal afferents are first-order or second-order neurons, and furthermore, whether various other cell types such as laryngeal taste cells, solitary chemosensory cells, neuroendocrine cells, or other epithelial or immune cell types may play an upstream role.

Here, we used molecular and genetic approaches to provide insights into sensory pathways that protect the upper airways. Single-cell RNA sequencing revealed a remarkable diversity of vagal afferents, and Cre mice were obtained for genetic control over most neuron subtypes individually or in small clusters, enabling links between cell identity, terminal morphology, sensory response, and physiological function. Cell-type-specific optogenetics revealed that rare vagal P2RY1 neurons (~100 per mouse) elicit a suite of airway protective responses including expiratory reflexes, vocal fold adduction, apnea, and fictive swallow. Moreover, ablation of vagal P2RY1 neurons impairs defensive responses to laryngeal challenges from acid and water, but not salt or force. Genetically guided anatomical tracing revealed that vagal P2RY1 neurons densely innervate laryngeal epithelium, closely apposing laryngeal taste buds. Laryngeal chemosensory reflexes are mimicked by optogenetic activation of epithelial cells, and are lost in knockout mice lacking ionotropic purinergic receptors. Thus, Cre-guided mapping, optogenetics, and cell ablation provide evidence that one of ~37 identified vagal cell subtypes functions as a second-order sensor for specific chemical threats in the larynx.

RESULTS

Reflexes Evoked by Laryngeal Stimulation

Swallowing is a complex motor action with distinct oral, pharyngeal, and esophageal phases (Steele and Miller, 2010). The pharyngeal phase of swallowing plays an active role in airway defense by clearing infiltrate away from the airways while propelling food, water, and other ingested contents safely past the larynx into the esophagus. (Pharyngeal swallow is also termed "secondary swallow" when initiated in the absence of an oral phase.) Chemical and mechanical stimulation of the larynx evokes guarding reflexes like apnea, vocal fold adduction, and laryngeal vestibule closure, and also clearance reflexes like pharyngeal swallow and cough. The same sensory stimulus can variably evoke a pharyngeal swallow, persistent apnea, and cough, with responses differing across species, age, depth of anesthesia, and stimulus magnitude (Nishino et al., 1990; Troche et al., 2014). The contributions of different laryngeal chemoreceptors and mechanoreceptors in these complex sensorimotor transitions are not well understood.

To monitor airway defense reflexes, we developed an *in vivo* preparation in anesthetized mice to record swallowing responses to laryngeal stimuli (Figure 1B). Solutions were introduced at a very slow rate (100 μL/min) through a cannula inserted past the tongue and directly over the larynx, with an exit port placed in the trachea below the vocal folds. A tracheal pressure transducer was inserted below the exit port to monitor breathing rhythms. Evoked swallows were quantified by visually observing hyoid elevation and were not observed under baseline conditions involving continuous slow perfusion of saline (PBS). Furthermore, based on control trials with PBS, swallowing was not evoked by flow alterations that may be associated with switching perfusion solutions. We found that robust and repetitive swallowing was evoked by transient perfusion of several test stimuli through the larynx, including water, acid, and high salt (Figures 1C and 1D). Swallowing was also evoked by mechanical stimulation of the larynx by direct physical probing. In contrast, laryngeal perfusion of TRPA1 or TRPV1 agonists, as well as bitter, sweet, or umami tastants (dissolved in PBS) did not evoke pharyngeal swallows.

Water, high salt, and acid also evoked transient apneas with each swallow, as well as occasional expiratory reflexes (Figure 1C). An airway expiratory reflex is a sudden forced airway evacuation reminiscent of a cough, but unlike a cough is not associated with a prior deep inspiration (Ludlow, 2015). Transection of the SLN eliminated swallowing to laryngeal water, acid, and high salt, and decreased the frequency of force-evoked swallow, consistent with a key role for larynx-innervating neurons (Figure 1E). Together, these findings reveal at least four modalities of upper airway stimuli that evoke reflexive secondary swallow: water, acid, high salt, and force. Thus, chemosensory responses in the larynx can be robustly elicited in mice and are at least partially distinct from classical taste responses of gustatory nerves.

Evoking Fictive Swallows by Sensory Neuron Optogenetics

We used optogenetics to identify sensory neurons involved in airway defense. The throat is densely innervated by the vagus and glossopharyngeal nerves, and in mice afferent soma from these nerves form a pair of fused nodose/jugular/petrosal (NJP) superganglia, each containing ~2,300 sensory neurons clustered near the jugular foramen at the base of the skull (Fox et al., 2001). We crossed mice harboring a Cre-dependent Channelrhodopsin allele (*loxP-ChR2*) to *Vglut2-ires-Cre* and

Chat-ires-Cre mice, which respectively label the vast majority of sensory and motor fibers in vagal and glossopharyngeal nerves. Optogenetic stimulation was achieved in offspring by focal illumination of the vagus nerve trunk or particular nerve branches (Figure 1F).

Activating all vagal sensory neurons in *Vglut2-ires-Cre; loxP-ChR2* mice evoked repetitive swallowing (Figure 1G; Video S1), with an average of 4.3 swallows per 10-s photostimulation trial. Pharyngeal swallows were observed and distinguished from primary swallows based on a lack of tongue movement and from esophageal swallows based on a lack of esophageal peristalsis. These findings indicate that pharyngeal swallow can be separately initiated and controlled, even under anesthesia. Pharyngeal swallows were further distinguished from other potential throat movements (such as cough or gaping), as they were associated with transient increases in pharyngeal pressure, contraction of the digastric muscle (that elevates the hyoid bone) as recorded by electromyography (EMG), and laryngeal elevation (Figure 1F). Analysis of tracheal pressure also revealed a transient apnea that occurred with each optogenetically evoked swallow (Figures 1F and 1G).

Bulk optogenetic stimulation of NJP sensory neurons, in addition to evoking swallow, also evoked occasional airway expiratory reflexes (1.5 events per 10-s trial) (Figures 1F and 1G). Expiratory reflexes sometimes occurred immediately after a swallow and other times were observed as isolated events. Light-evoked swallows and expiratory reflexes were not observed in control *loxP-ChR2* mice or during vagal motor neuron stimulation in *Chat-ires-Cre; loxP-ChR2* mice because motor control of these reflexes is conveyed by other efferent nerves.

Sweeping Genetic Control over Vagal Sensory Neuron Subtypes

We next defined NJP sensory neurons involved in airway protection. We used single-cell RNA sequencing for unbiased investigation of sensory neuron diversity in the vagus and glossopharyngeal nerves (Figure 2A). Sensory neurons were acutely harvested from NJP ganglia of wild-type (8-week-old, male, C57BL6/J) mice, enriched by centrifugation in a Percoll gradient and encapsulated in nanoliter droplets containing primer-decorated beads for barcoded cDNA synthesis. Single-cell cDNA was then amplified and sequenced to generate single-cell transcriptomes.

Transcriptome data (average: 6,937 unique reads spanning 2,293 genes) were obtained on 46,712 cells, including 25,117 sensory neurons as well as macrophages, stromal cells, and various types of glial cells (Figures S1A–S1C). Sensory neurons were defined based on expression of several neuronal markers, including *Vglut2* (*Slc17a6*), a glutamate transporter expressed in >99% of vagal and glossopharyngeal sensory neurons but not in other non-neuronal cell types of sensory ganglia (Chang et al., 2015). Unsupervised clustering analysis revealed ~37 classes of sensory neurons (Figure 2B), each ranging in size from 12 to 151 neurons per NJP ganglion (Figure S1C). Additional rare vagal sensory neuron subtypes were uncovered here, compared with other recent single-cell sequencing studies (Bai et al., 2019; Kupari et al., 2019; Mazzone et al., 2020), likely because of the larger number of cells we analyzed. 27 cell clusters, representing 79% of NJP sensory neurons (19,756/25,117), were derived from nodose and inferior petrosal ganglia based on expression of *Phox2b*, a marker for epibranchial placode-derived sensory neurons (Figure S1D). The remaining 10 clusters, representing 21% of neurons, did not express *Phox2b* but instead expressed *Prdm12*, a neural crest transcription factor and marker for sensory neurons of the jugular and superior glossopharyngeal ganglia. Markers that broadly distinguish petrosal neurons from nodose/jugular neurons are not available, although at least one large placode-derived neuron cluster (NP9) lacks expression of *Hoxb4* (Figure S1D), and is likely part of the glossopharyngeal nerve.

We defined cell clusters by singular or combinatorial expression of signature genes (Figure 2C); see Table S1 for signature genes used to define each cell cluster. *In situ* hybridization verified expression of selected markers in dispersed subsets of sensory neurons (Figure 2D). Gene Ontology (GO) term analysis on differentially expressed genes revealed that sensory neuron subtypes differed primarily by expression of various cell surface receptors such as G protein-coupled receptors (GPCRs), ion channels such as TRPs and PIEZOs, and neuropeptides (Figures S1D and S1E). Single-cell transcriptome data of vagal/glossopharyngeal sensory neurons are publicly available (GEO: GSE145216).

The 37 classes of NJP sensory neurons may differ with regard to organ-targeting pattern, response property, and/or physiological function. We previously characterized various classes of sensory neurons that innervate the lungs, stomach, intestine, and aorta, and differentially control breathing, heart rate, blood pressure, and gut motility (Chang et al., 2015; Min et al., 2019; Williams et al., 2016). For example, in the digestive system, stomach and intestine mechanoreceptors express several gut hormone receptors and are marked in *Glp1r-ires-Cre* mice (Williams et al., 2016); cell clusters that express *Glp1r* include NP4, NP8, NP26, and NP27. Other sensory neurons marked in *Gpr65-ires-Cre* mice function as chemosensory neurons that innervate intestinal villi and stomach mucosa (Williams et al., 2016), with *Gpr65* highly expressed in cluster NP5. Some vagal afferents in the lung and lower airways contain PIEZO2, sense airway stretch, and evoke a classic apnea reflex termed the Hering-Breuer inspiratory reflex (Nonomura et al., 2017). There are multiple classes of PIEZO2 neurons (Figure 3A), and it is unclear which transcriptome-defined cluster detects airway stretch, and which others may mediate different internal senses such as arterial baroreception (Min et al., 2019; Zeng et al., 2018). Some vagal P2RY1 neurons also innervate the lung, with arbors that appose clusters of lung secretory cells termed neuroepithelial bodies (Chang et al., 2015).

Single-cell sequencing revealed that visceral sensations of the vagus and glossopharyngeal nerves depend on a striking diversity of cell types. This estimate of cell diversity is conservative, and some co-clustered cells may perform similar sensory functions such as mechanosensation or cytokine detection in different organs. Thus, recognized cell type diversity may be even greater once physiological roles are understood for each neuron group. Moreover, most vagal and glossopharyngeal neuron subtypes have not been accessed previously through selective genetic approaches.

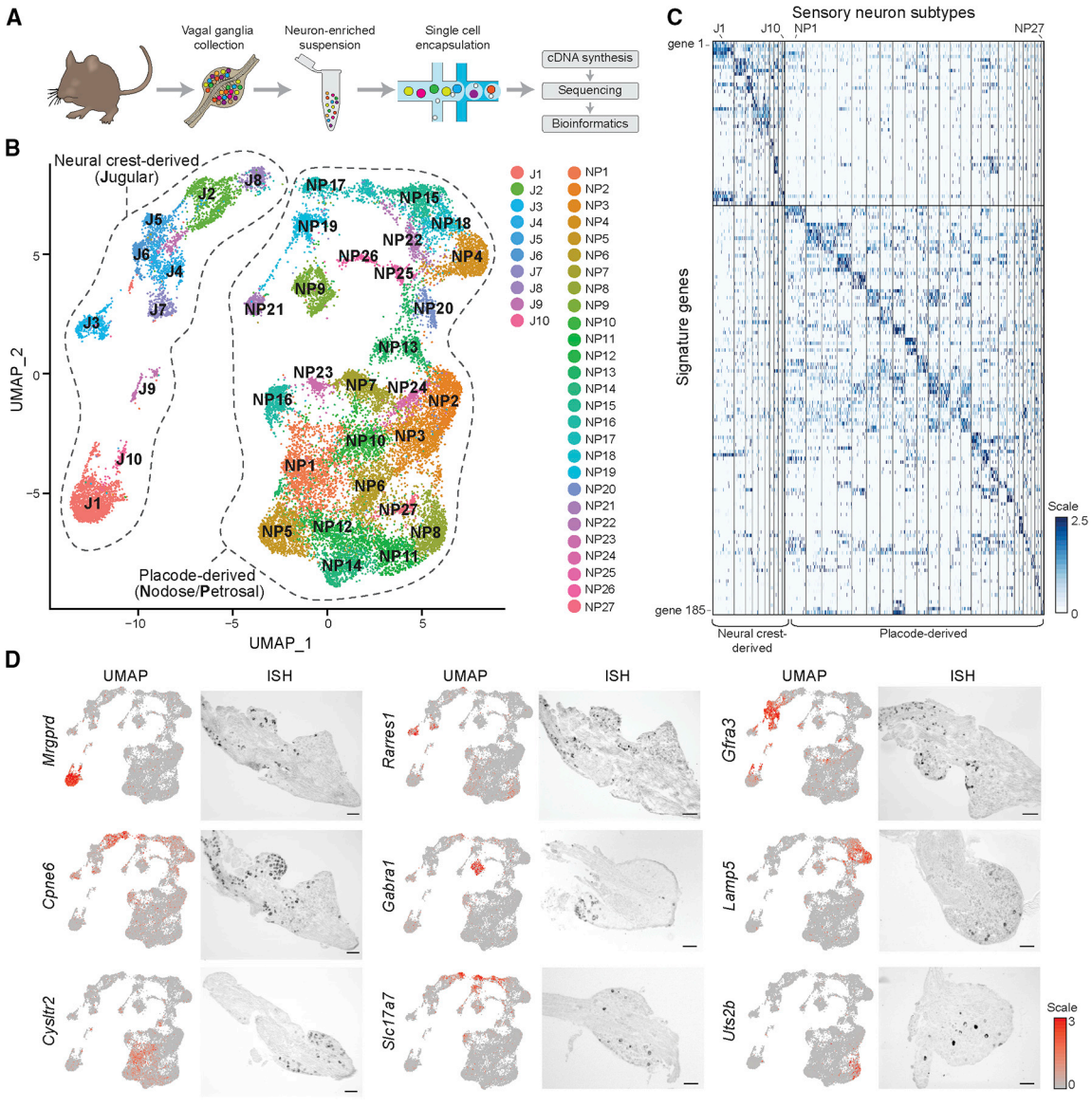

Figure 2. An Atlas of Sensory Neuron Subtypes from Vagal and Glossopharyngeal Nerves

(A) Experimental pipeline for single-cell transcriptome analysis.

(B) Uniform manifold approximation and projection (UMAP) plots indicating cell subtype diversity across 25,117 NJP sensory neurons. Neuron clusters from jugular (J1–J10) and nodose/petrosal (NP1–NP27) ganglia are color coded.

(C) Normalized expression levels (blue-gray scale) of cluster-defining signature genes (see Table S1 for genes 1–185) across all NJP sensory neurons analyzed.

(D) UMAP plots from single-cell transcriptomes (left) and RNA *in situ* hybridization in cryosections of NJP ganglia (right) showing gene expression in sensory neuron subsets. Scale bars, 100 μm.

See also Figure S1 and Table S1.

To obtain genetic control over newly identified NJP sensory neuron subtypes, we constructed *Gabra1-ires-Cre* and *Crhr2-ires-Cre* mice; two-color analysis validated that Cre recombinase drove reporter expression to the correct neurons in these mice (Figure S2). We also obtained other published mouse lines, *Calb1-ires-Cre* and *Npy1r-Cre* mice, and observed that they target subsets of NJP sensory neurons. Together with knockin lines we previously reported to target NJP ganglia (*P2ry1-ires-Cre*, *Gpr65-ires-Cre*, *Glp1r-ires-Cre*, *Piezo2-ires-Cre*, and *Npy2r-ires-Cre* mice), this genetic toolkit provides access to 33 out of the 37 NJP neuronal populations, with each Cre line marking different small groups of neurons (Figure 3). Moreover, cell types co-labeled by one Cre line are often differentially labeled by a second Cre line; for example, NP17 is labeled by *Piezo2-ires-Cre* and *P2ry1-ires-Cre*, NP18 is labeled by *Piezo2-ires-Cre* but not *P2ry1-ires-Cre*, and NP19 is labeled by *P2ry1-ires-Cre* but not *Piezo2-ires-Cre*. By using this large panel of Cre lines, and treating each Cre line as an independent linear

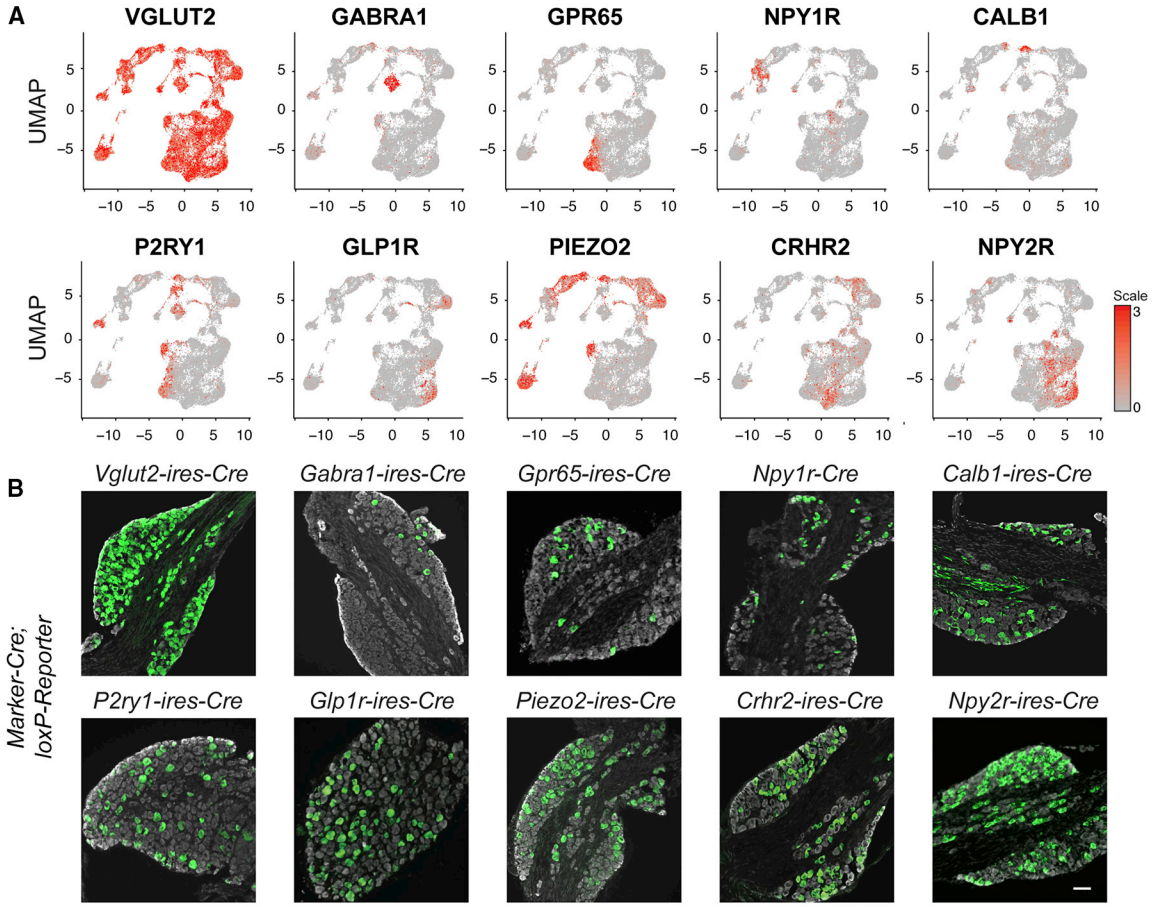

Figure 3. A Genetic Toolkit for Accessing Small Groups of NJP Sensory Neurons

(A) UMAP plots indicating expression of genes in NJP sensory neurons.

(B) Native reporter fluorescence in cryosections of NJP ganglia from mice with Cre alleles and Cre-dependent reporter genes (*L10-GFP*, except *tdTomato* for *Calb1-ires-Cre* and *Vglut-ires-Cre*). tdTomato images were pseudocolored to match GFP images; far-red fluorescent Nissl counterstain (gray). Scale bar, 100 μm. The image from *Npy2r-ires-Cre* mice was previously published (Chang et al., 2015).

See also Figure S2.

variable, we reasoned that it could be possible to deduce the functions of particular transcriptome-defined sensory neurons.

Vagal P2RY1 Neurons Evoke a Coordinated Airway Defense Program

We used optogenetics to identify NJP sensory neuron subtypes that evoke swallowing. We crossed *loxP-ChR2* mice to *Calb1-ires-Cre*, *Piezo2-ires-Cre*, *Gabra1-ires-Cre*, *Gpr65-ires-Cre*, *Npy1r-Cre*, *Npy2r-ires-Cre*, *Crhr2-ires-Cre*, *Glp1r-ires-Cre*, and *P2ry1-ires-Cre* mice that label different groups of sensory neurons, and wild-type mice for control experiments. Optogenetic stimulation was achieved in offspring by focal illumination of the nerve trunk or particular nerve branches.

Light-induced stimulation of vagal P2RY1 neurons evoked frequent pharyngeal swallowing and expiratory reflexes (5.7 and 3.0 per 10-s stimulation) (Figures 4A and 4B). Swallows occurred (maximal likelihood) with a latency of 0.67 s after optogenetic stimulation and an interswallow interval of 1.65 s. Both reflexes were evoked by branch-selective optogenetics involving focal SLN illumination in *P2ry1-ires-Cre; loxP-ChR2* mice, but not pharyngeal or glossopharyngeal nerve illumination, indicating involvement of laryngeal neurons (Figure S3A). Furthermore, optogenetic stimulation of vagal P2RY1 neurons in a vagus nerve stump above a trunk transection, but not below, induced swallowing, demonstrating a role for sensory neurons; additionally, responses persisted after bilateral transection of SLN motor neurons (trunk transection below the illumination point with contralateral SLN transection), consistent with a role for non-vagal motor neurons (Figure S3B). Swallows and expiratory reflexes were more rarely observed following optogenetic activation of vagal NPY1R neurons, and were never observed following stimulation of vagal PIEZO2, CALB1, GABRA1, CRHR2, GPR65, NPY2R, or GLP1R neurons (Figures 4A and 4B).

Based on prior RNA *in situ* hybridization analysis, *P2ry1* is expressed in 11.6% of NJP sensory neurons, or ~250 neurons per ganglion (Chang et al., 2015). Single-cell RNA sequencing data indicated abundant levels of *P2ry1* transcript in five neuron subtypes (J3, NP16, NP17, NP19, and NP26) and lower levels in

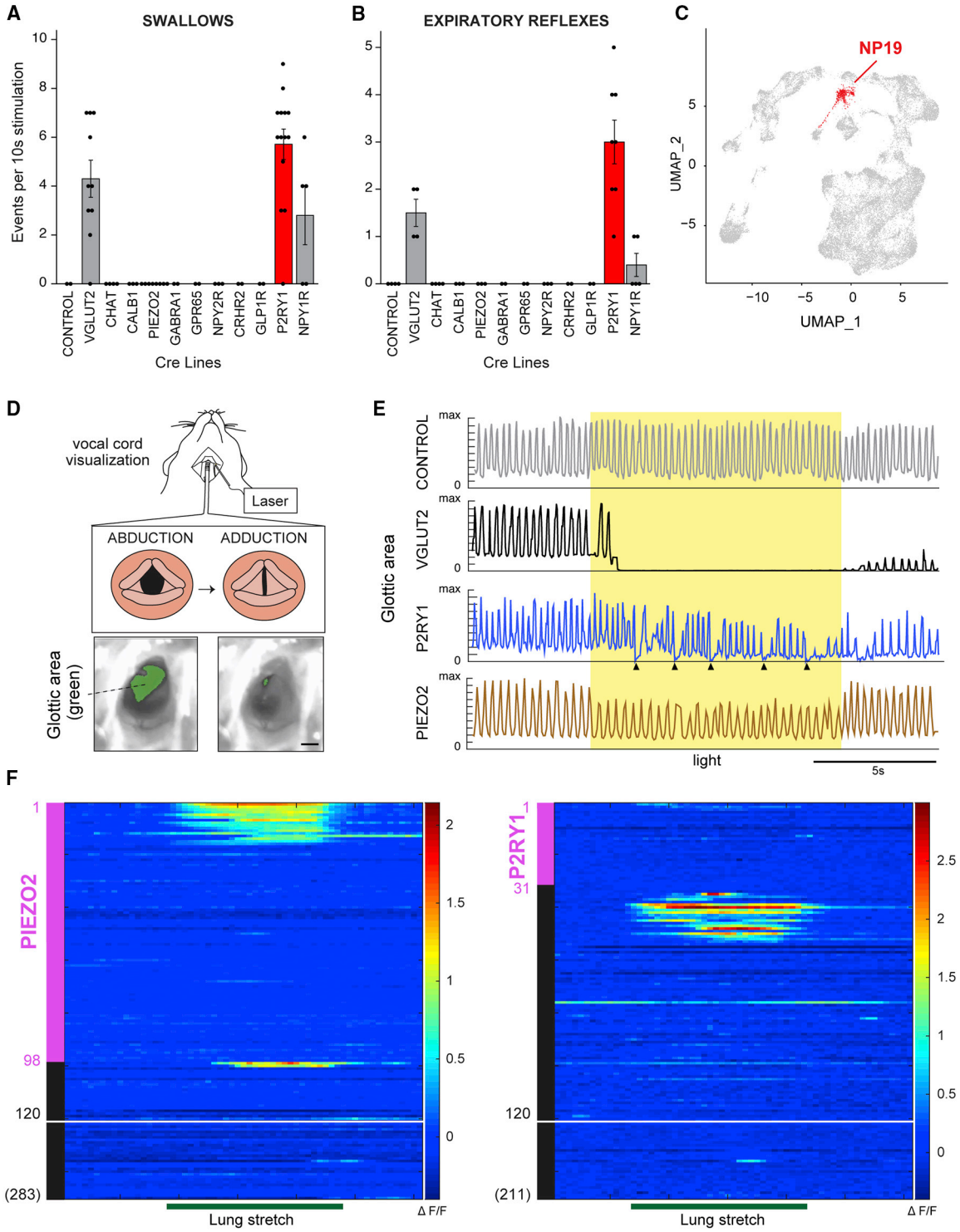

Figure 4. P2RY1 Neurons Elicit a Multifaceted Airway Defense Program

(A and B) Swallows (A) and expiratory reflexes (B) were counted during vagus nerve optogenetics experiments in mice expressing ChR2 from Cre drivers indicated, n = 2–14 mice, mean ± SEM.

(C) UMAP plot indicating NP19 neurons, which are the only neurons that express *P2ry1*, but not *Piezo2*, *Crhr2*, *Gpr65*, or *Gabra1*.

(D) Cartoon (top) depicting vocal fold dynamics, with images (bottom) of glottic area (green) during abduction and adduction. Scale bar, 500 μm.

(E) Representative graphs of glottic area over time during (yellow shading) vagus nerve optogenetics; triangles: swallows.

(legend continued on next page)

four other neuron subtypes (NP5, NP9, NP13, and NP23). Four of these nine P2RY1 neuron subtypes also express *Piezo2* (J3, NP16, NP17, and NP26), and all of them except for NP19 express *Piezo2*, *Crhr2*, *Gpr65*, and/or *Gabra1*. Eight of nine P2RY1 neuron populations are targeted by Cre lines that do not evoke swallowing, pinpointing a particular P2RY1-expressing cell subtype, NP19 neurons (~50 neurons per NJP ganglion), as a candidate mediator of laryngeal reflexes (Figure 4C). Single-cell sequencing of NP19 neurons revealed expression of *Phox2b*, indicating placodal origin, signature genes that include *P2ry1*, *Slc18a3*, *Gm2990*, *Runx3*, and *Pappa2* (Figure S3C), but not *Trpa1* or *Trpv1*, which are implicated in irritant responses.

Airway challenges evoke coordinated motor responses that also include vocal fold adduction and breathing inhibition, so we asked whether activating vagal P2RY1 neurons evoked these additional hallmarks of airway defense. Vocal fold adduction provides a physical barrier to prevent passage of threatening substances from the larynx to the trachea (Jadcherla et al., 2010). The vocal folds were visualized with a miniaturized fiber endoscope (Video S2) or by light microscopy (Figure 4D), and normal glottic movements were observed across the respiratory cycle, including full abduction during inspiration and partial adduction during expiration. Optogenetic activation of all vagal sensory neurons in *Vglut2-ires-Cre; loxP-ChR2* mice induced sustained and complete glottic closure, while activating P2RY1 or PIEZO2 neurons differentially controlled vocal fold dynamics (Figure 4E). Light-induced stimulation of vagal P2RY1 neurons caused brief, sporadic episodes of complete glottic closure that were synchronized with each swallow. For comparison, optogenetic activation of PIEZO2 neurons decreased the extent of glottic abduction during inspiratory events, without changing the extent of glottic adduction during expiratory events. These findings indicate that vagal P2RY1 neurons evoke episodes of complete vocal fold adduction, a stereotyped signature of airway protection.

Laryngeal challenges also suppress respiration to prevent unintended aspiration of foreign materials into the lungs and upper airways. We noted above that optogenetic activation of P2RY1 neurons caused a transient apnea that occurred with each swallow. Under deeper anesthesia, stimulating P2RY1 or VGLUT2 neurons no longer evoked frequent swallowing, but instead caused a prolonged apnea and reduction in minute volume (Figure S4), as reported previously (Chang et al., 2015). The observation that physiological responses (swallow, cough, or apnea) vary with depth of anesthesia is consistent with previously reported anesthesia-dependent responses mediated by the SLN (Nishino et al., 1990). We note that multiple classes of apnea-promoting neurons were identified by optogenetics under deep anesthesia (Chang et al., 2015; Nonomura et al., 2017), including neurons that express PIEZO2 and function as airway stretch sensors. ~50% of vagal P2RY1 neurons co-express PIEZO2, and optogenetic activation of vagal P2RY1 neurons also inhibits respiration (Chang et al., 2015). It is possible that airway stretch sensors are encompassed by both *Piezo2-ires-Cre* mice and *P2ry1-ires-Cre* mice; however, activating PIEZO2 neurons did not evoke swallowing and associated transient apnea under lighter anesthesia, nor expiratory reflexes, suggesting that vagal P2RY1 and PIEZO2 neurons mediate distinct apnea-related reflexes.

To exclude the possibility that P2RY1-evoked apnea is related to airway stretch reception, we imaged calcium transients in individual genetically defined neurons of vagal ganglia (Figure 4F). We generated *P2ry1-ires-Cre; loxP-tdTomato; ROSA26-GCaMP3* (*P2ry1-GCaMP** mice) and *Piezo2-ires-Cre; loxP-tdTomato; ROSA26-GCaMP3* (*Piezo2-GCaMP** mice), in which all vagal sensory neurons express GCaMP3 from a constitutive promoter and Cre-expressing cells also express tdTomato. We then imaged single-cell calcium transients in NJP ganglia during trials of airway stretch stimulation, as described previously (Williams et al., 2016). Sensory neurons responsive to airway stretch were rare, dispersed, and marked by tdTomato expression in *Piezo2-GCaMP** mice (17/19 responsive neurons), but not in *P2ry1-GCaMP** mice (2/23 responsive neurons). Thus, airway stretch sensation is mediated by PIEZO2-positive, P2RY1-negative sensory neurons. Together, these findings reveal separate subtypes of apnea-promoting vagal afferents that can be distinguished using genetic tools. Vagal PIEZO2 neurons mediate airway stretch-induced apnea, while vagal P2RY1 neurons instead evoke a coordinated motor program with multiple signatures of airway defense, including not only apnea, but also vocal fold adduction, pharyngeal swallowing, and expiratory reflexes.

Ablation of Vagal P2RY1 Neurons Eliminates Laryngeal Responses to Airway Challenge

Optogenetic activation of P2RY1 neurons evokes a suite of protective reflexes similar to those elicited by various airway threats. We next used targeted neuron ablation to ask whether P2RY1 neurons are required for physiological responses to any particular laryngeal challenge. Targeted ablation of NJP sensory neurons was achieved using Cre-based expression of diphtheria toxin receptor (DTR), as reported previously (Min et al., 2019; Tränkner et al., 2014). Mouse cells are normally resistant to diphtheria toxin (DT), but can be rendered sensitive by expression of DTR (Saito et al., 2001). We generated *P2ry1-ires-Cre; loxP-DTR* mice and injected DT bilaterally into NJP ganglia (*P2ry1-ABLATE* mice), resulting in efficient ablation of vagal P2RY1 neurons, while sparing other intermingled NJP sensory neurons (Figures 5A and S5). To control for non-specific ablation, we also injected DT into NJP ganglia of *loxP-DTR* mice lacking a Cre driver (DT-injected control mice), as well as *Npy1r-Cre; loxP-DTR* (*Npy1r-ABLATE*) and *Gabra1-ires-Cre; loxP-DTR* (*Gabra1-ABLATE*) mice.

Next, we asked whether swallowing responses to various airway assaults were intact in *P2ry1-ABLATE* mice using our *in vivo* preparation for laryngeal perfusion where we observed

(F) *In vivo* calcium imaging in NJP ganglia from 5 *Piezo2-GCaMP** mice (left) and 3 *P2ry1-GCaMP** mice (right). Rows indicate responses (ΔF/F, color scale) over time of individual neurons to lung stretch (15 s). Magenta and black bars represent tdTomato-positive and negative neurons. Not all unresponsive tdTomato-negative neurons are depicted; numbers at y axis base indicate total number of viable imaged neurons.
See also Figures S3 and S4.

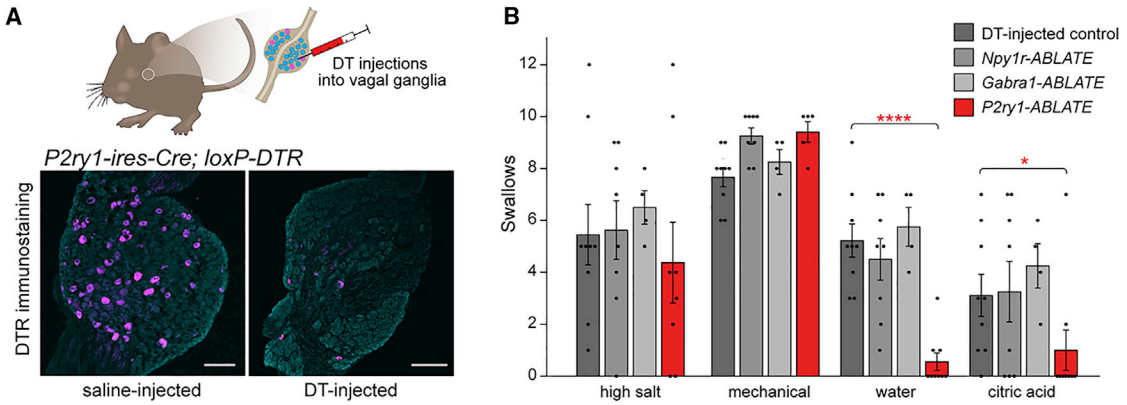

Figure 5. P2RY1 Neurons Mediate Responses to Laryngeal Water and Acid Challenge

(A) Cartoon (top) of DT-mediated ablation of Cre-expressing cells. DTR immunostaining (magenta) of NJP ganglia from *P2ry1-ires-Cre; loxP-DTR* mice 3 weeks after intraganglionic saline (left) or DT (right) injection, far-red fluorescent Nissl counterstain (gray). Scale bars, 100 μm.

(B) Swallows over 20 s perfusion or 10 mechanical trials in mice indicated, n = 4–9 mice, mean ± SEM, *p < 0.05, **p < 0.005, ****p < 0.00005.

See also Figure S5.

responses to water, acid, high salt, and force. We found that *P2ry1-ABLATE* mice, but not other mice analyzed, had impaired swallowing responses to both laryngeal acid and water (Figure 5B). However, swallowing to laryngeal force and high salt was normal in *P2ry1-ABLATE* mice, with levels similar to control mice, *Npy1r-ABLATE* mice, and *Gabra1-ABLATE* mice. These findings indicate that laryngeal P2RY1 neurons are required for sensing specific chemosensory challenges to upper airway integrity.

Vagal P2RY1 Neurons Densely Innervate Laryngeal Taste Buds

Many types of laryngeal terminals have been described, but those that mediate specific aspects of airway defense are unknown due to a lack of genetic tools. Next, we asked whether vagal P2RY1 neurons might innervate the larynx, and if so, whether they form particular terminal structures.

We previously developed a genetic approach to trace the anatomical projections of Cre-expressing vagal sensory neurons (Chang et al., 2015; Min et al., 2019; Williams et al., 2016). Cre-dependent Adeno-associated viruses (AAVs) encoding fluorescent (*AAV-flex-tdTomato*) or alkaline phosphatase (*AAV-flex-AP*) reporters were directly injected into NJP ganglia of Cre knockin mice, and labeled fibers subsequently visualized in peripheral tissues (Figure 6A). Bulk labeling of NJP sensory neurons using Cre-independent AAVs or Cre-dependent AAVs in *Vglut2-ires-Cre* mice revealed a complex network of neuronal terminals throughout the larynx, with particularly dense innervation of the epithelium of the epiglottis, arytenoids, vocal folds, and subglottis underneath the thyroid cartilage. Diverse terminal morphologies were congested and intermingled across the laryngeal surface, explaining the prior challenges of linking terminal morphology to physiological function.

We next surveyed the types of upper airway terminals that could be selectively marked using specific Cre lines. We injected NJP ganglia of *Npy1r-Cre*, *Npy2r-ires-Cre*, *Calb1-ires-Cre*, *Piezo2-ires-Cre*, *Gabra1-ires-Cre*, and *P2ry1-ires-Cre* mice bilaterally with reporter AAVs and visualized neuronal endings in the larynx. In each of these six mouse lines, labeled neurites densely innervated the larynx (Figures 6C and S6A), while neurites labeled by similar approaches in *Gpr65-ires-Cre* mice did not. Moreover, CALB1, P2RY1, NPY1R, and NPY2R neurons formed different terminal types in laryngeal epithelium (Figure 6D). CALB1 neurons displayed striking chandelier-shaped terminals concentrated on the ciliated epithelium of the epiglottis and subglottis below the thyroid cartilage. NPY1R and NPY2R neurons, which are transcriptionally distinct subsets of TRPV1 neurons predominantly derived from jugular and nodose ganglia respectively, formed free endings in different airway regions: NPY1R terminals were observed in epiglottis, arytenoids, and trachea, while NPY2R terminals were only found in the trachea up to the cricoid cartilage and not in the vocal folds or above. PIEZO2 and GABRA1 neurons did not access the epithelium, but instead formed distinct subepithelial endings. PIEZO2 fibers encircled laryngeal mucosal glands, and also ramified within intrinsic laryngeal muscles, while GABRA1 neurons displayed large, isolated, and branched terminals in the trachealis muscle.

Next, we focused on anatomical characterization of vagal P2RY1 neurons, given their role as laryngeal chemoreceptors. Vagal P2RY1 neurons deposited dense and complex neuronal arbors in ciliated epithelium, including the laryngeal surface of the epiglottis and subglottis, and more dispersed and distinctive endings in squamous epithelium near the vocal folds, arytenoid cartilages, and aryepiglottal folds (Figure 6B and S6B). The terminals of P2RY1 neurons in squamous epithelium formed rare, characteristic corpuscles of ~40 μm diameter (Figure 6E). Interestingly, P2RY1 neuron corpuscles directly apposed laryngeal taste buds, as visualized by immunohistochemistry for the taste cell marker KRT8 (Figures 6F and 6G). Every P2RY1 corpuscle in the larynx appeared to innervate a taste bud, and quantitative analysis revealed that the majority of taste buds (33/46, 6 mice) were innervated by a P2RY1 corpuscle; this is likely an underestimation of taste bud innervation based on the partial efficiency of AAV infection (~60%) in NJP ganglion

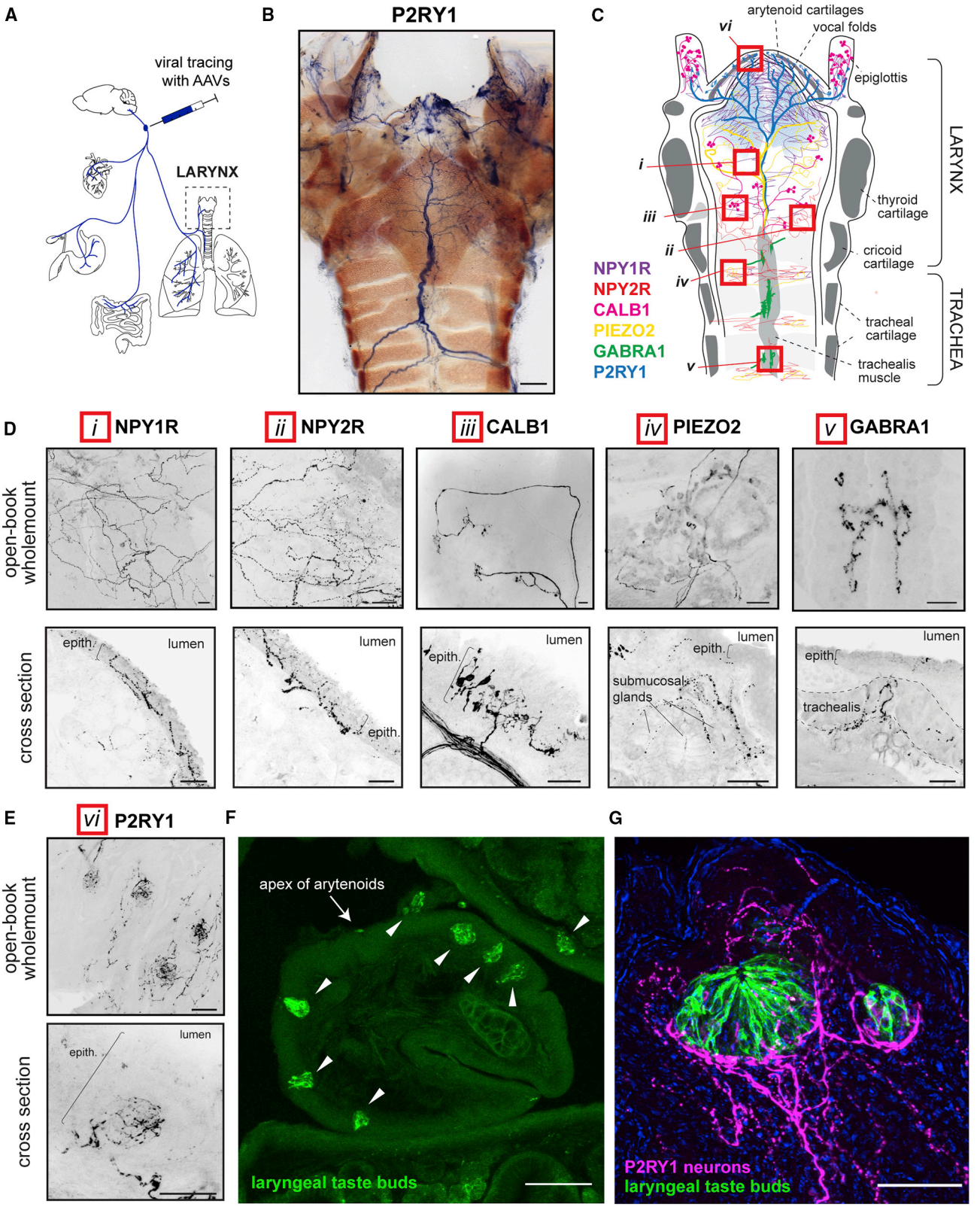

(legend on next page)

neurons. We also note that some P2RY1 terminals, presumably from the pharyngeal branch of the glossopharyngeal nerve, contacted taste buds in the oropharynx, as well as lingual taste buds in foliate and circumvallate papillae (Figure S6C). Together, these observations suggest that vagal P2RY1 neurons function as second-order chemosensory neurons in the larynx and in other locations.

Epithelial Cells as Primary Sentinels for Airway Defense

Lingual afferents that mediate bitter, sweet, sour, umami, and salt taste are second-order neurons that receive input from dedicated taste cells on the tongue (Yarmolinsky et al., 2009). In the larynx, it has been debated whether water and acid sensation occurs in upstream sentinel cells or directly by neurons, and adding complexity, multiple laryngeal sensory pathways have been proposed for both stimuli (Harding et al., 1978; Kollarik and Undem, 2002; Sant'Ambrogio et al., 1991). We observed that vagal P2RY1 neurons innervate laryngeal epithelium including taste buds, and are also required for physiological responses to laryngeal acid and water challenge. These findings raise the possibility that upstream sentinel cells first detect water and/or acid in the larynx, and relay information to P2RY1 neurons through specific neurotransmitters. We next sought to test this model by both stimulating and blocking epithelial cell-to-neuron communication.

First, we asked whether optogenetic stimulation of epithelial cells in the larynx triggered airway defense responses. We generated *Krt8-Cre^{ER}; loxP-ChR2* mice, which drives Channelrhodopsin expression broadly in ciliated epithelium and selectively to laryngeal taste buds within squamous epithelium (Figure 7A); reporter expression was not observed in vagal sensory neurons (Figures S7A and S7B). Optogenetic stimulation of epithelial cells in different throat regions was achieved by selective optic fiber positioning (Figure 7B). Light-evoked swallowing was observed by illumination of the larynx (light directed toward the inferior edge of the arytenoids and vocal folds), but not the upper trachea (between thyroid and cricoid cartilages) or posterior oral cavity (Figure 7C). Swallowing was also not evoked by illuminating NJP ganglia in *Krt8-Cre^{ER}; loxP-ChR2* mice. Together, these findings suggest that stimulation of upstream epithelial cells in the larynx is sufficient to activate the neural arc resulting in secondary swallow.

Next, we asked whether eliminating epithelial cell-neuron communication blocks physiological responses to particular laryngeal stimuli. Lingual taste cells communicate with second-order gustatory fibers using ATP as a neurotransmitter, and responses to sweet, salty, sour, bitter, and umami tastants are disrupted in knockout mice lacking the ionotropic ATP receptors *P2x2* and *P2x3* (Finger et al., 2005). P2X3-immunoreactive nerve terminals are abundant in laryngeal epithelium (Takahashi et al., 2016); moreover, *P2x2* and *P2x3* are highly expressed in NP19 neurons, the P2RY1 neuron subset implicated by optogenetics experiments to be involved in laryngeal defense (Figure S7C), raising the possibility that certain laryngeal sensations require ATP signaling as well. We measured swallowing to laryngeal challenge in *P2x2/P2x3* knockout mice, and observed that although responses to laryngeal force and high salt were normal, responses to acid were diminished, and responses to laryngeal water were lost (Figures 7D and 7E). Thus, activation of laryngeal epithelial cells is sufficient to evoke swallowing, while knockout of ionotropic ATP receptors impairs swallowing responses to particular laryngeal stimuli. We also noted that water responses were intact in mice lacking phospholipase C β2 (PLCβ2) (Figure S7D); PLCβ2 is utilized by solitary chemosensory cells as well as taste cells that detect sweet, bitter, and umami chemicals, but not salty or sour chemicals (Krasteva et al., 2011; Zhang et al., 2003). Together, these findings indicate that certain chemical challenges in the larynx are first detected by epithelial sentinel cells and then communicated to P2RY1 neurons (NP19 neurons) through ATP, ultimately evoking a suite of defensive responses including apnea, vocal fold adduction, and pharyngeal swallow.

DISCUSSION

Ingested food and drink pass directly over the airways *en route* to the esophagus. The larynx is a critical sensory hotspot for neuronal detection of airway threats and coordination of defensive reflexes to secure airway integrity. Vagal sensory neurons display a multitude of sensory terminals in the larynx, but their functions have been difficult to disentangle without specific genetic reagents. Here, we used single-cell RNA sequencing and a large genetic toolkit to interrogate the cellular diversity of vagal and glossopharyngeal nerves. Cre-guided sensory neuron mapping, ablation, and optogenetics revealed that a small cluster of P2RY1 neurons mediates a suite of stereotyped airway protection responses that include pharyngeal swallow, apnea, expiratory reflexes, and vocal fold adduction. Moreover, P2RY1 neurons form corpuscular terminals that appose laryngeal taste buds, and physiological responses to laryngeal water challenge involve epithelial sentinel cells and ATP signaling.

Each mouse NJP ganglion is small, with ~2,300 neurons, yet rich in diversity, with ~37 molecularly distinct sensory neuron

Figure 6. P2RY1 Neurons Innervate Laryngeal Taste Buds

(A) Cartoon depicting Cre-based anatomical mapping of vagal sensory neurons.

(B) P2RY1 neuron terminals visualized in an open-book preparation of the larynx after injecting *AAV-flex-AP* into NJP ganglia of *P2ry1-ires-Cre* mice. Scale bar, 500 μm.

(C) Diagram depicting terminals of various neuron types in the larynx after AAV mapping. Red boxes *i* to *vi* show regions of larynx highlighted below.

(D) Representative images of terminals formed by neuron subtypes captured by wholemount analysis of an open-book preparation (top) or in larynx cryosections (bottom) following tdTomato immunostaining. Scale bars, 50 μm.

(E) Representative images of P2RY1 terminals, as depicted in (D). Scale bars, 50 μm.

(F) Taste buds visualized in larynx cryosections by KRT8 immunohistochemistry (green). Scale bar, 100 μm.

(G) Two-color immunohistochemistry for KRT8 (green) and tdTomato (magenta) in cryosections of larynx from *P2ry1-ires-Cre* mice injected with *AAV-flex-tdTomato* in NJP ganglia. Scale bar, 50 μm.

See also Figure S6.

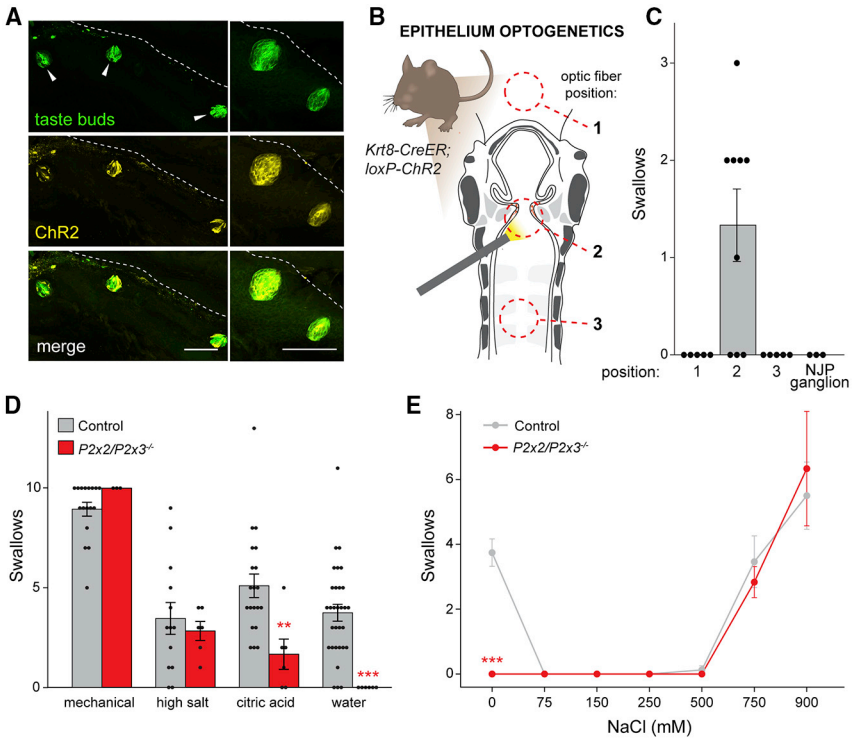

Figure 7. Laryngeal Reflexes Involve Epithelial Cell-Neuron Communication

(A) Two-color immunohistochemistry for KRT8 (green) and eYFP (yellow) in cryosections of arytenoid epithelium from tamoxifen-treated *Krt8-Cre^{ER}; loxP-ChR2* mice (*ChR2* encodes a ChR2-YFP fusion protein). Scale bars, 100 μm.

(B) Cartoon of epithelium optogenetics in *Krt8-Cre^{ER}; loxP-ChR2* mice, with illumination of oral cavity (1), larynx (2), trachea (3), or NJP ganglion.

(C) Swallows per optogenetics trial (10 Hz) in tamoxifen-treated *Krt8-Cre^{ER}; loxP-ChR2* mice (n = 3–9, mean ± SEM), with light fiber positions indicated in (B).

(D) Swallows evoked in wild-type (control, n = 13–31) and *P2x2/P2x3$^{-/-}$* mice (n = 6) by test stimuli, mean ± SEM, $^{**}p < 0.005$, $^{***}p < 5 \times 10^{-10}$.

(E) Swallows evoked in wild-type (control) and *P2x2/P2x3$^{-/-}$* mice by laryngeal perfusion (20 s) of NaCl solutions of various concentration in water, n = 8–31 control mice, 3–6 *P2x2/P2x3$^{-/-}$* mice, mean ± SEM, $^{**}p < 0.005$, $^{***}p < 5 \times 10^{-10}$.

See also Figure S7.

subtypes. This cellular diversity is presumably needed as the vagus nerve innervates vast terrain, projecting to many internal organs within the body, and detects an assortment of sensory cues. Our findings also suggest that a small number of vagal sensory neurons may be sufficient to mediate a particular physiological function; for example, there are only ~50 NP19 neurons in each ganglion devoted to an aspect of airway defense. For comparison, the somatosensory system is much larger in mice, involving hundreds of thousands of sensory neurons located across numerous dorsal root ganglia (DRG) (Gjerstad et al., 2002). Single-cell sequencing of DRG neurons revealed various neuron subtypes involved in touch, pain, proprioception, temperature sensation, and itch (Li et al., 2016; Usoskin et al., 2015). The dramatic increase in the total number of DRG neurons presumably enables highly specific spatial discrimination of sensory stimuli, which may not be needed for at least some vagally mediated internal organ sensations. Other sensory systems rely on a smaller number of input channels; in the visual system, there are a few principal sensory cells: rods, cones, and melanopsin-utilizing retinal ganglion cells, while the gustatory system involves five classical taste modalities—sweet, salty, sour, bitter, and umami (Yarmolinsky et al., 2009). At the other extreme, the olfactory system contains >1,000 sensory receptors in mice and has the power to detect and discriminate a tremendous diversity of odors (Buck and Axel, 1991). The number of sensations mediated by the vagus nerve has not previously been quantified, but is presumably large based on the underlying cellular diversity. Furthermore, it seems likely that some sensory neurons characterized here mediate internal organ sensory functions that have yet to be determined. Approaches used here provide a technical blueprint for studying the roles of sensory neurons in other aspects of interoception.

Among the many unresolved questions in interoception, laryngeal cell types and terminal morphologies that sense water have remained elusive. We observed numerous terminal structures in the larynx that can be distinguished using various Cre lines, including epithelial chandelier terminals, corpuscular terminals, and free endings, as well as terminals in muscle and around submucosal glands. The sensory functions of most laryngeal terminal types remain unclear. Several prior studies proposed that water was directly sensed in the larynx by first-order free nerve endings rather than specialized terminal structures, although direct functional perturbations were lacking (Anderson et al., 1990; Storey and Johnson, 1975). Here, we present several pieces of evidence demonstrating that a physiological response to laryngeal water instead involves second-order neurons that communicate with upstream epithelial sentinel cells. Genetically guided anatomical mapping revealed that vagal P2RY1 neurons form large corpuscular terminals that appose laryngeal taste buds, which are marked in *Krt8-Cre^{ER}; loxP-ChR2* mice. Ablation of vagal P2RY1 neurons, or knockout of ionotropic ATP receptors, eliminates defensive responses to laryngeal water challenge. Furthermore, optogenetic stimulation of vagal P2RY1 neurons, or laryngeal epithelial cells, evokes hallmarks of airway defense. Based on these findings, we posit that airway epithelial cells first detect water, and then communicate with second-order P2RY1 afferents through ATP action to relay the signal centrally. We do note that SLN nerve responses to water and acid reportedly persist in *P2x2/P2x3* knockout mice (Ohkuri et al., 2012), raising the possibility that additional detection pathways exist for these cues, perhaps with relevance for distinct physiological effects.

ATP is utilized as a neurotransmitter by lingual taste buds for communication with afferent nerves (Finger et al., 2005), and

may serve a similar epithelial cell-neuron communication role in other organs, such as the skin, bladder, and carotid body (Cockayne et al., 2000; Dussor et al., 2009; Piskuric and Nurse, 2013). Here, we show that in the larynx, a water-evoked reflex also requires ionotropic ATP signaling. The functions of laryngeal taste buds have been mysterious, and findings here raise them to be prime candidates involved in airway protection. A recent study proposed that water sensation can occur through sour taste cells in the oral cavity, as marked by *Pkd2l1* expression (Zocchi et al., 2017); however, we note that laryngeal water responses did not require bicarbonate washout, that secondary swallowing was not evoked by optogenetic stimulation of glossopharyngeal neurons that innervate lingual taste buds, and that *Pkd2l1* could potentially mark discrete taste cells in the larynx. Other classes of epithelial sentinel cells could additionally (1) be innervated by P2RY1 neurons, (2) be targeted in *Krt8-Cre^{ER}; loxP-ChR2* mice, and (3) utilize ATP as a neurotransmitter. Other rare airway epithelial cells include solitary chemosensory cells and neuroendocrine cells. Solitary chemosensory cells express bitter taste receptors that detect irritants, including bacterial molecules involved in quorum sensing, and in response, mediate respiratory depression (Finger et al., 2005; Krasteva et al., 2011). However, bitter receptor agonists administered in the larynx do not evoke swallow, water-evoked swallow persists in *Plcβ2* knockout mice, and solitary chemosensory cells reportedly utilize acetylcholine rather than ATP to communicate with afferent nerves.

Multiple chemosensory pathways emanate from the larynx and are relevant for airway defense. Pathogen sensation is proposed to involve not only upstream epithelial cells, but also direct engagement of sensory neurons, for example through formyl peptide receptors or Mas-related G protein-coupled receptors (MRGs) (Chiu et al., 2013; Han et al., 2018). Airway irritants include cigarette smoke, inhaled dust, TRPA1-activating oxidants such hypochlorite and hydrogen peroxide, and the TRPV1 agonist capsaicin (Bessac and Jordt, 2008; Bessac et al., 2008; Canning et al., 2004). Single-cell RNA sequencing indicated that vagal NP19 neurons are nodose-derived, and distinct from sensory neurons that express TRPA1, TRPV1, or MRGs; Channelrhodopsin-assisted conduction velocity measurements also indicated that most P2RY1 neurons are A fibers (Chang et al., 2015) distinct from classical nociceptive C fibers. We note that rarer swallowing was observed following activation of NPY1R neurons, a jugular population that does express both TRPA1 and TRPV1. Furthermore, a population of P2RY1-negative neurons is sufficient to mediate salt sensation; laryngeal salt responses occur at a much higher stimulus threshold (750 mM) (Figure 7E) than appetitive salt taste responses (3–30 mM) (Ishiwatari and Bachmanov, 2012) and also do not require P2X2/P2X3, suggesting distinct sensory pathways for oral and laryngeal salt sensation. Together, there appear to be various chemosensory neurons in the upper airways responsible for detecting pathogens, respiratory irritants, and airway challenges from ingested or refluxed food and drink.

Sensorimotor transformations underlying airway protection have been poorly defined, as linking specific reflexes to particular laryngeal neurons is technically challenging in the absence of genetic tools. One model is that various sensory stimuli engage separate information processing streams to mediate different motor responses. Alternatively, various airway challenges might engage common brain command centers that provide a general alarm signal and orchestrate multiple components of a stereotyped motor program (Jean, 2001). The observation that distinct laryngeal challenges (water, acid, high salt, and force) evoke similar physiological reactions (cough, apnea, pharyngeal swallow, and vocal fold adduction) suggests that at least some sensory inputs might converge in responding neural circuits. Here, optogenetic stimulation of a small cluster of transcriptionally defined vagal sensory neurons (NP19 neurons) is sufficient to evoke multiple aspects of airway defense. We observe that motor control centers apparently evoke the command to swallow in a probabilistic manner, with a refractory period between swallows. AAV-based mapping of vagal P2RY1 axons previously revealed preferential innervation of lateral subdivisions within the nucleus of the solitary tract (NTS) in the brainstem (Chang et al., 2015), and NTS neurons display polymodal responses to certain mechanical and chemical stimuli in the larynx (Takagi et al., 1995). However, it is debated whether different sensory neuron subtypes converge in the NTS, or whether polymodality arises earlier in the periphery. Single unit studies in laryngeal afferent nerves reported a continuous response spectrum including both multimodal and unimodal responses, with the frequency of polymodal responses varying across studies (Smith and Hanamori, 1991; Storey, 1968; Takagi et al., 1995). Here, we observed that ablation of P2RY1 neurons impairs responses to challenge from laryngeal water and acid, but not to challenges from high salt or force, indicating that a functional division of labor does exist between at least some sensory neurons in the periphery.

Optogenetic studies revealed distinct classes of apnea-promoting vagal afferents. Vagal PIEZO2 neurons mediate lower airway stretch-induced apnea (Nonomura et al., 2017), a classical reflex termed the Hering Breuer inspiratory reflex, while vagal P2RY1 neurons instead induce apnea as part of an upper airway protective motor program. Other NJP afferents also likely cause apnea, including esophageal distension receptors that protect the airways during acid reflux and vomiting, as well as pharyngeal mechanoreceptors (Lang et al., 2001; Shaker and Hogan, 2000). Yet other NJP sensory neurons instead enhance respiration, such as carotid body-innervating chemoreceptors (Chang, 2017). Thus, respiratory control centers can be differentially toggled by various afferent pathways from vagal and glossopharyngeal nerves.

Stimulating vagal P2RY1 neurons also evokes expiratory reflexes, forced airway evacuations that help expel infiltrate and are nicknamed "laryngeal coughs" (Ludlow, 2015). While mice do not display audible coughing behavior, laryngeal water and acid sensation potently produce cough in other species, including humans (Canning et al., 2004). Because mouse sensory neurons can detect laryngeal stimuli that evoke cough in other species, one model is that sensory pathways for airway threats such as those described here are evolutionarily conserved between mouse and human, even if evoked motor programs have diverged. Consistent with this model, human and mouse contain a similar diversity of laryngeal taste cells (Jetté et al., 2020). It is thus intriguing to note that we observed

a loss of physiological responses to laryngeal water perfusion in *P2x2/P2x3* knockout mice. The P2X3 antagonist AF-219 is an effective suppressant of chronic cough in human patients, although mechanisms have been elusive (Abdulqawi et al., 2015). One prior explanation for AF-219 antitussive action involved blockade of ATP-mediated inflammatory signals that may chronically sensitize cough receptors (Abdulqawi et al., 2015). Data here suggest an alternative model that P2X antagonism directly disrupts laryngeal sensation by some vagal afferents through inhibition of epithelial cell-neuron communication. Multiple types of cough neurons have been proposed, including both A and C fibers with varying sensitivity to capsaicin and anesthetics (Canning et al., 2004; Mazzone and Undem, 2016). Consistent with the notion of multiple afferent pathways for cough, proposed cough receptor terminals in the trachea are distinct from the corpuscular terminals of P2RY1 neurons described here. We note that laryngeal responses to water were lost following P2RY1 neuron ablation and *P2x2/P2x3* knockout, but responses to force and high salt were not, further indicating multiple types of airway protection neurons. Because knockout of ionotropic ATP receptors does not block activity of all laryngeal defense pathways, AF-219 may very well have more efficacy as a cough suppressant in some patients than others, depending on which sensory pathways are sensitized or chronically engaged. Understanding the diversity of airway sensory neurons, and which pathways go awry across patient populations, should help optimize clinical treatments.

In addition to chronic cough, persistent or impaired activity in laryngeal sensory neurons can cause other severe clinical problems. Persistent engagement of laryngeal water receptors causes reflexive cough and/or swallowing in adults (Canning et al., 2004; Shingai et al., 1989), but in newborn animals (puppies, kittens, and lambs) causes an unadapting apnea which can be fatal if the offending stimulus is not removed (Boggs and Bartlett, 1982; Kovar et al., 1979). In human babies, physical obstruction or fluid accumulation in the larynx may similarly cause unrelenting engagement of airway defense pathways, and seemingly has the potential to cause a sustained apnea that results in sudden infant death syndrome (SIDS). At the other extreme, breakdown of airway protection leads to respiratory infections such as aspiration pneumonia, which is among the leading causes of death in the elderly. Loss of laryngeal sensory neuron function also causes dysphagia and associated weight loss, speech impairments, and risk of choking, and severely impacts quality of life. Understanding the diversity of airway sensory neurons, and mechanisms by which they function, may provide new insights into human physiology in health and disease.

STAR★METHODS

Detailed methods are provided in the online version of this paper and include the following:

- KEY RESOURCES TABLE
- LEAD CONTACT AND MATERIALS AVAILABILITY
- EXPERIMENTAL MODEL AND SUBJECT DETAILS
- METHOD DETAILS
  - Single-cell RNA sequencing
  - Generating Cre knock-in mice
  - Optogenetics
  - Physiological measurements
  - Larynx perfusions
  - *In situ* hybridization
  - Histology and immunochemistry
  - Calcium imaging in vagal ganglia
  - Cell ablations and nerve transections
  - AAV-guided anatomical mapping
- QUANTIFICATION AND STATISTICAL ANALYSIS
- DATA AND CODE AVAILABILITY

SUPPLEMENTAL INFORMATION

Supplemental Information can be found online at https://doi.org/10.1016/j.cell.2020.03.004.

ACKNOWLEDGMENTS

We thank David Ginty, Jay Rajagopal, Isaac Chiu, John Flanagan, Rui Chang, Phillip Song, and Marie Bao for manuscript comments; Brad Lowell for mice; and David Strochlic for images. Silvia Huerta and Yandan Wang assisted with anatomical analysis, Jian Shu and Eric Lander with pilot single-cell RNA sequencing, Eli Weinstein with analyzing vocal fold dynamics, the HMS Nikon Imaging Center with microscopy, the Boston Children's Hospital Mouse Gene Manipulation Core with making mice, and the HMS Biopolymers Facility with single-cell sequencing. The work was supported by NIH (DP1 AT009497 and R01 HL132255 to S.D.L., F31 HL132645 to B.D.U., and F30 CA177170 to E.K.W.), a Faculty Scholars Award from the Howard Hughes Medical Institute (to S.D.L.), and an American Diabetes Association postdoctoral fellowship (to R.D.B.). S.L.P. is an Open Philanthropy Fellow of the Life Sciences Research Foundation. S.D.L. is an investigator of the Howard Hughes Medical Institute.

AUTHOR CONTRIBUTIONS

S.L.P., B.D.U., and S.D.L. designed the study. S.L.P. performed sequencing. S.L.P. and R.D.B. generated Cre lines. S.L.P. and B.D.U. performed optogenetics, neuron ablations, and physiological measurements. E.K.W. performed ganglion imaging. S.L.P. and B.D.U. performed anatomical tracing. S.L.P., B.D.U., and S.D.L. wrote the manuscript.

DECLARATION OF INTERESTS

S.D.L. is a consultant for Kallyope.

Received: November 18, 2019
Revised: February 8, 2020
Accepted: March 4, 2020
Published: April 6, 2020

REFERENCES

Abdulqawi, R., Dockry, R., Holt, K., Layton, G., McCarthy, B.G., Ford, A.P., and Smith, J.A. (2015). P2X3 receptor antagonist (AF-219) in refractory chronic cough: a randomised, double-blind, placebo-controlled phase 2 study. Lancet *385*, 1198–1205.

Anderson, J.W., Sant'Ambrogio, F.B., Mathew, O.P., and Sant'Ambrogio, G. (1990). Water-responsive laryngeal receptors in the dog are not specialized endings. Respir. Physiol. *79*, 33–43.

Bai, L., Mesgarzadeh, S., Ramesh, K.S., Huey, E.L., Liu, Y., Gray, L.A., Aitken, T.J., Chen, Y., Beutler, L.R., Ahn, J.S., et al. (2019). Genetic Identification of Vagal Sensory Neurons That Control Feeding. Cell *179*, 1129–1143.

Baral, P., Umans, B.D., Li, L., Kirschbaum, T., Wei, Y., Zhou, Y., Yipp, B.G., Liberles, S.D., and Chiu, I.M. (2018). Nociceptor sensory neurons suppress

neutrophil and gamma delta T cell responses in bacterial lung infections and lethal pneumonia. Nat. Med. *24*, 417–426.

Bessac, B.F., and Jordt, S.E. (2008). Breathtaking TRP channels: TRPA1 and TRPV1 in airway chemosensation and reflex control. Physiology (Bethesda) *23*, 360–370.

Bessac, B.F., Sivula, M., von Hehn, C.A., Escalera, J., Cohn, L., and Jordt, S.E. (2008). TRPA1 is a major oxidant sensor in murine airway sensory neurons. J. Clin. Invest. *118*, 1899–1910.

Boggs, D.F., and Bartlett, D., Jr. (1982). Chemical specificity of a laryngeal apneic reflex in puppies. J. Appl. Physiol. *53*, 455–462.

Bolser, D.C. (1991). Fictive cough in the cat. J. Appl. Physiol. (1985) *71*, 2325–2331.

Buck, L., and Axel, R. (1991). A novel multigene family may encode odorant receptors: a molecular basis for odor recognition. Cell *65*, 175–187.

Butler, A., Hoffman, P., Smibert, P., Papalexi, E., and Satija, R. (2018). Integrating single-cell transcriptomic data across different conditions, technologies, and species. Nat. Biotechnol. *36*, 411–420.

Canning, B.J., Mazzone, S.B., Meeker, S.N., Mori, N., Reynolds, S.M., and Undem, B.J. (2004). Identification of the tracheal and laryngeal afferent neurones mediating cough in anaesthetized guinea-pigs. J. Physiol. *557*, 543–558.

Chang, A.J. (2017). Acute oxygen sensing by the carotid body: from mitochondria to plasma membrane. J. Appl. Physiol. (1985) *123*, 1335–1343.

Chang, R.B., Strochlic, D.E., Williams, E.K., Umans, B.D., and Liberles, S.D. (2015). Vagal Sensory Neuron Subtypes that Differentially Control Breathing. Cell *161*, 622–633.

Chen, E.Y., Tan, C.M., Kou, Y., Duan, Q., Wang, Z., Meirelles, G.V., Clark, N.R., and Ma'ayan, A. (2013). Enrichr: interactive and collaborative HTML5 gene list enrichment analysis tool. BMC Bioinformatics *14*, 128.

Chiu, I.M., Heesters, B.A., Ghasemlou, N., Von Hehn, C.A., Zhao, F., Tran, J., Wainger, B., Strominger, A., Muralidharan, S., Horswill, A.R., et al. (2013). Bacteria activate sensory neurons that modulate pain and inflammation. Nature *501*, 52–57.

Cockayne, D.A., Hamilton, S.G., Zhu, Q.M., Dunn, P.M., Zhong, Y., Novakovic, S., Malmberg, A.B., Cain, G., Berson, A., Kassotakis, L., et al. (2000). Urinary bladder hyporeflexia and reduced pain-related behaviour in P2X3-deficient mice. Nature *407*, 1011–1015.

Coleridge, H.M., Coleridge, J.C., and Schultz, H.D. (1989). Afferent pathways involved in reflex regulation of airway smooth muscle. Pharmacol. Ther. *42*, 1–63.

Doty, R.W. (1951). Influence of stimulus pattern on reflex deglutition. Am. J. Physiol. *166*, 142–158.

Dussor, G., Koerber, H.R., Oaklander, A.L., Rice, F.L., and Molliver, D.C. (2009). Nucleotide signaling and cutaneous mechanisms of pain transduction. Brain Res. Brain Res. Rev. *60*, 24–35.

Feindel, W. (1956). The neural pattern of the epiglottis. J. Comp. Neurol. *105*, 269–285.

Finger, T.E., Danilova, V., Barrows, J., Bartel, D.L., Vigers, A.J., Stone, L., Hellekant, G., and Kinnamon, S.C. (2005). ATP signaling is crucial for communication from taste buds to gustatory nerves. Science *310*, 1495–1499.

Fox, E.A., Phillips, R.J., Baronowsky, E.A., Byerly, M.S., Jones, S., and Powley, T.L. (2001). Neurotrophin-4 deficient mice have a loss of vagal intraganglionic mechanoreceptors from the small intestine and a disruption of short-term satiety. J. Neurosci. *21*, 8602–8615.

Gjerstad, M.D., Tandrup, T., Koltzenburg, M., and Jakobsen, J. (2002). Predominant neuronal B-cell loss in L5 DRG of p75 receptor-deficient mice. J. Anat. *200*, 81–87.

Han, L., Limjunyawong, N., Ru, F., Li, Z., Hall, O.J., Steele, H., Zhu, Y., Wilson, J., Mitzner, W., Kollarik, M., et al. (2018). Mrgprs on vagal sensory neurons contribute to bronchoconstriction and airway hyper-responsiveness. Nat. Neurosci. *21*, 324–328.

Harding, R., Johnson, P., and McClelland, M.E. (1978). Liquid-sensitive laryngeal receptors in the developing sheep, cat and monkey. J. Physiol. *277*, 409–422.

Ishiwatari, Y., and Bachmanov, A.A. (2012). NaCl taste thresholds in 13 inbred mouse strains. Chem. Senses *37*, 497–508.

Jadcherla, S.R., Hogan, W.J., and Shaker, R. (2010). Physiology and pathophysiology of glottic reflexes and pulmonary aspiration: from neonates to adults. Semin. Respir. Crit. Care Med. *31*, 554–560.

Jafari, S., Prince, R.A., Kim, D.Y., and Paydarfar, D. (2003). Sensory regulation of swallowing and airway protection: a role for the internal superior laryngeal nerve in humans. J. Physiol. *550*, 287–304.

Jean, A. (2001). Brain stem control of swallowing: neuronal network and cellular mechanisms. Physiol. Rev. *81*, 929–969.

Jetté, M.E., Clary, M.S., Prager, J.D., and Finger, T.E. (2020). Chemical receptors of the arytenoid: A comparison of human and mouse. Laryngoscope *130*, 423–430.

Kollarik, M., and Undem, B.J. (2002). Mechanisms of acid-induced activation of airway afferent nerve fibres in guinea-pig. J. Physiol. *543*, 591–600.

Kovar, I., Selstam, U., Catterton, W.Z., Stahlman, M.T., and Sundell, H.W. (1979). Laryngeal chemoreflex in newborn lambs: respiratory and swallowing response to salts, acids, and sugars. Pediatr. Res. *13*, 1144–1149.

Krasteva, G., Canning, B.J., Hartmann, P., Veres, T.Z., Papadakis, T., Mühlfeld, C., Schliecker, K., Tallini, Y.N., Braun, A., Hackstein, H., et al. (2011). Cholinergic chemosensory cells in the trachea regulate breathing. Proc. Natl. Acad. Sci. USA *108*, 9478–9483.

Kuleshov, M.V., Jones, M.R., Rouillard, A.D., Fernandez, N.F., Duan, Q., Wang, Z., Koplev, S., Jenkins, S.L., Jagodnik, K.M., Lachmann, A., et al. (2016). Enrichr: a comprehensive gene set enrichment analysis web server 2016 update. Nucleic Acids Res. *44*, W90–W97.

Kupari, J., Haring, M., Agirre, E., Castelo-Branco, G., and Ernfors, P. (2019). An Atlas of Vagal Sensory Neurons and Their Molecular Specialization. Cell Rep. *27*, 2508–2523.

Lang, I.M., Medda, B.K., and Shaker, R. (2001). Mechanisms of reflexes induced by esophageal distension. Am. J. Physiol. Gastrointest. Liver Physiol. *281*, G1246–G1263.

Li, C.L., Li, K.C., Wu, D., Chen, Y., Luo, H., Zhao, J.R., Wang, S.S., Sun, M.M., Lu, Y.J., Zhong, Y.Q., et al. (2016). Somatosensory neuron types identified by high-coverage single-cell RNA-sequencing and functional heterogeneity. Cell Res. *26*, 967.

Ludlow, C.L. (2015). Laryngeal Reflexes: Physiology, Technique, and Clinical Use. J. Clin. Neurophysiol. *32*, 284–293.

Mazzone, S.B., and Undem, B.J. (2016). Vagal Afferent Innervation of the Airways in Health and Disease. Physiol. Rev. *96*, 975–1024.

Mazzone, S.B., Tian, L., Moe, A.A.K., Trewella, M.W., Ritchie, M.E., and McGovern, A.E. (2020). Transcriptional Profiling of Individual Airway Projecting Vagal Sensory Neurons. Mol. Neurobiol. *57*, 949–963.

Min, S., Chang, R.B., Prescott, S.L., Beeler, B., Joshi, N.R., Strochlic, D.E., and Liberles, S.D. (2019). Arterial baroreceptors sense blood pressure through decorated aortic claws. Cell Rep. *29*, 2192–2201.

Montmayeur, J.P., Liberles, S.D., Matsunami, H., and Buck, L.B. (2001). A candidate taste receptor gene near a sweet taste locus. Nat. Neurosci. *4*, 492–498.

Mu, L., and Sanders, I. (2000). Sensory nerve supply of the human oro- and laryngopharynx: a preliminary study. Anat. Rec. *258*, 406–420.

Nishino, T., Hiraga, K., and Yokokawa, N. (1990). Laryngeal and respiratory responses to tracheal irritation at different depths of enflurane anesthesia in humans. Anesthesiology *73*, 46–51.

Nonomura, K., Woo, S.H., Chang, R.B., Gillich, A., Qiu, Z., Francisco, A.G., Ranade, S.S., Liberles, S.D., and Patapoutian, A. (2017). Piezo2 senses airway stretch and mediates lung inflation-induced apnoea. Nature *541*, 176–181.

Oh, S.W., Harris, J.A., Ng, L., Winslow, B., Cain, N., Mihalas, S., Wang, Q., Lau, C., Kuan, L., Henry, A.M., et al. (2014). A mesoscale connectome of the mouse brain. Nature *508*, 207–214.

Ohkuri, T., Horio, N., Stratford, J.M., Finger, T.E., and Ninomiya, Y. (2012). Residual chemoresponsiveness to acids in the superior laryngeal nerve in "taste-blind" (P2X2/P2X3 double-KO) mice. Chem. Senses *37*, 523–532.

Piskuric, N.A., and Nurse, C.A. (2013). Expanding role of ATP as a versatile messenger at carotid and aortic body chemoreceptors. J. Physiol. *591*, 415–422.

R Core Team (2019). R: A language and environment for statistical computing (Vienna, Austria: R Foundation for Statistical Computing). https://www.R-project.org/.

Saito, M., Iwawaki, T., Taya, C., Yonekawa, H., Noda, M., Inui, Y., Mekada, E., Kimata, Y., Tsuru, A., and Kohno, K. (2001). Diphtheria toxin receptor-mediated conditional and targeted cell ablation in transgenic mice. Nat. Biotechnol. *19*, 746–750.

Sampson, S., and Eyzaguirre, C. (1964). Some Functional Characteristics of Mechanoreceptors in the Larynx of the Cat. J. Neurophysiol. *27*, 464–480.

Sant'Ambrogio, G., Anderson, J.W., Sant'Ambrogio, F.B., and Mathew, O.P. (1991). Response of laryngeal receptors to water solutions of different osmolality and ionic composition. Respir. Med. *85* (*Suppl. A*), 57–60.

Santoso, L.F., Kim, D.Y., and Paydarfar, D. (2019). Sensory dysphagia: A case series and proposed classification of an under recognized swallowing disorder. Head Neck *41*, E71–E78.

Shaker, R., and Hogan, W.J. (2000). Reflex-mediated enhancement of airway protective mechanisms. Am. J. Med. *108* (*Suppl 4a*), 8S–14S.

Shingai, T., Miyaoka, Y., Ikarashi, R., and Shimada, K. (1989). Swallowing reflex elicited by water and taste solutions in humans. Am. J. Physiol. *256*, R822–R826.

Smith, D.V., and Hanamori, T. (1991). Organization of gustatory sensitivities in hamster superior laryngeal nerve fibers. J. Neurophysiol. *65*, 1098–1114.

Steele, C.M., and Miller, A.J. (2010). Sensory input pathways and mechanisms in swallowing: a review. Dysphagia *25*, 323–333.

Storey, A.T. (1968). A functional analysis of sensory units innervating epiglottis and larynx. Exp. Neurol. *20*, 366–383.

Storey, A.T., and Johnson, P. (1975). Laryngeal water receptors initiating apnea in the lamb. Exp. Neurol. *47*, 42–55.

Takagi, S., Umezaki, T., and Shin, T. (1995). Convergence of laryngeal afferents with different natures upon cat NTS neurons. Brain Res. Bull. *38*, 261–268.

Takahashi, N., Nakamuta, N., and Yamamoto, Y. (2016). Morphology of P2X3-immunoreactive nerve endings in the rat laryngeal mucosa. Histochem. Cell Biol. *145*, 131–146.

Tizzano, M., Gulbransen, B.D., Vandenbeuch, A., Clapp, T.R., Herman, J.P., Sibhatu, H.M., Churchill, M.E., Silver, W.L., Kinnamon, S.C., and Finger, T.E. (2010). Nasal chemosensory cells use bitter taste signaling to detect irritants and bacterial signals. Proc. Natl. Acad. Sci. USA *107*, 3210–3215.

Tränkner, D., Hahne, N., Sugino, K., Hoon, M.A., and Zuker, C. (2014). Population of sensory neurons essential for asthmatic hyperreactivity of inflamed airways. Proc. Natl. Acad. Sci. USA *111*, 11515–11520.

Travers, S.P., and Nicklas, K. (1990). Taste bud distribution in the rat pharynx and larynx. Anat. Rec. *227*, 373–379.

Troche, M.S., Brandimore, A.E., Godoy, J., and Hegland, K.W. (2014). A framework for understanding shared substrates of airway protection. J. Appl. Oral Sci. *22*, 251–260.

Usoskin, D., Furlan, A., Islam, S., Abdo, H., Lönnerberg, P., Lou, D., Hjerling-Leffler, J., Haeggström, J., Kharchenko, O., Kharchenko, P.V., et al. (2015). Unbiased classification of sensory neuron types by large-scale single-cell RNA sequencing. Nat. Neurosci. *18*, 145–153.

Williams, E.K., Chang, R.B., Strochlic, D.E., Umans, B.D., Lowell, B.B., and Liberles, S.D. (2016). Sensory Neurons that Detect Stretch and Nutrients in the Digestive System. Cell *166*, 209–221.

Yamamoto, Y., Hosono, I., Atoji, Y., and Suzuki, Y. (1997). Morphological study of the vagal afferent nerve endings in the laryngeal mucosa of the dog. Ann. Anat. *179*, 65–73.

Yarmolinsky, D.A., Zuker, C.S., and Ryba, N.J. (2009). Common sense about taste: from mammals to insects. Cell *139*, 234–244.

Zeng, W.Z., Marshall, K.L., Min, S., Daou, I., Chapleau, M.W., Abboud, F.M., Liberles, S.D., and Patapoutian, A. (2018). PIEZOs mediate neuronal sensing of blood pressure and the baroreceptor reflex. Science *362*, 464–467.

Zhang, Y., Hoon, M.A., Chandrashekar, J., Mueller, K.L., Cook, B., Wu, D., Zuker, C.S., and Ryba, N.J. (2003). Coding of sweet, bitter, and umami tastes: different receptor cells sharing similar signaling pathways. Cell *112*, 293–301.

Zocchi, D., Wennemuth, G., and Oka, Y. (2017). The cellular mechanism for water detection in the mammalian taste system. Nat. Neurosci. *20*, 927–933.

Please cite this article in press as: Prescott et al., An Airway Protection Program Revealed by Sweeping Genetic Control of Vagal Afferents, Cell (2020), https://doi.org/10.1016/j.cell.2020.03.004

STAR★METHODS

KEY RESOURCES TABLE

REAGENT or RESOURCE	SOURCE	IDENTIFIER
Antibodies		
Chicken anti-GFP	Abcam	Cat#ab13970; RRID:AB_300798
Rabbit anti-RFP	Rockland	Cat#600-401-379; RRID:AB_2209751
Goat anti-HB-EGF	R&D Systems	Cat#AF-259-NA; RRID:AB_354429
Rat anti-KRT8/TROMA-I	The Developmental Studies Hybridoma Bank	Cat#TROMA-I; RRID:AB_531826
Sheep anti-Digoxigenin, AP Conjugated	Roche	Cat#11093274910; RRID:AB_514497
Bacterial and Virus Strains		
AAV9.CAG.Flex.tdTomato.WPRE.BGH	Oh et al., 2014	Addgene viral prep #51503-AAV9
pENN.AAV.CB7.CI.eGFP.WPRE.rBG	James M. Wilson lab (unpublished)	Addgene viral prep #105542-AAV9
AAV9.CAG.flex.PLAP.WPRE.BGh	This paper	N/A
Critical Commercial Assays		
TSA Plus Cyanine 5.5 detection kit	Perkin-Elmer	SKU: NEL766001KT
MegaScript T7 kit	Invitrogen	Cat#AM1334
MegaScript SP6 kit	Invitrogen	Cat#AM1330
Chromium Single Cell 3′ GEM, Library & Gel Bead Kit v3	10x Genomics	PN-1000092
Chromium Single Cell B Chip Kit	10x Genomics	PN-1000154
Chromium i7 Multiplex Kit	10x Genomics	PN-120262
Deposited Data		
Single-cell RNaseq data	This study	GEO Accession ID: GSE145216
Quantitative data in figures	This study	Mendeley data https://doi.org/10.17632/4gfm8jp6dr.1
Experimental Models: Organisms/Strains		
Mouse: C57BL/6J	The Jackson Laboratory	Stock No: 000664
Mouse: B6;129S-*Calb1*$^{tm2.1(cre)Hze}$/J	The Jackson Laboratory	Stock No: 028532
Mouse: B6;129S6-*Chat*$^{tm2(cre)Lowl}$/J	The Jackson Laboratory	Stock No: 006410
Mouse: B6.Cg-Tg(RP23-268L19-EGFP)2Mik/J	The Jackson Laboratory	Stock No: 007902
Mouse: Tg(Krt8-cre/ERT2)17Blpn/J	The Jackson Laboratory	Stock No: 017947
Mouse: B6.Cg-*Npy1r*$^{tm1.1(cre/GFP)Rpa}$/J	The Jackson Laboratory	Stock No: 030544
Mouse: B6(SJL)-*Piezo2*$^{tm1.1(cre)Apat}$/J	The Jackson Laboratory	Stock No: 027719
Mouse: B6.129S1-*Plcb2*^{tm1Dwu}/J	The Jackson Laboratory	Stock No: 018064
Mouse: B6;129S6-*Gt(ROSA) 26Sor*$^{tm14(CAG-tdTomato)Hze}$/J	The Jackson Laboratory	Stock No: 007908
Mouse: B6;129S-*Gt(ROSA) 26Sor*$^{tm32(CAG-COP4*H134R/EYFP)Hze}$/J	The Jackson Laboratory	Stock No: 012569
Mouse: C57BL/6-*Gt(ROSA)26Sor*$^{tm1(HBEGF)Awai}$/J	The Jackson Laboratory	Stock No: 007900
Mouse: B6;129S-*Gt(ROSA)26Sor*$^{tm38(CAG-GCaMP3)Hze}$/J	The Jackson Laboratory	Stock No: 014538
Mouse: FVB/N-Tg(EIIa-cre)C5379Lmgd/J	The Jackson Laboratory	Stock No: 003314
Mouse: *Crhr2-ires-Cre*	This study	Deposited at Jax, Stock No: 033728
Mouse: *Gabra1-ires-Cre*	This study	N/A
Mouse: *Vglut2-ires-Cre*	The Jackson Laboratory	Stock No: 028863
Mouse: *loxP-L10-GFP*	Gift from Brad Lowell's lab	N/A
Mouse: *Glp1r*$^{tm1.1(cre)Lbrl}$/RcngJ	The Jackson Laboratory	Stock No: 029283

(*Continued on next page*)

Continued

REAGENT or RESOURCE	SOURCE	IDENTIFIER
Mouse: *P2ry1*$^{tm1.1(cre)Lbrl}$/RcngJ	The Jackson Laboratory	Stock No: 029284
Mouse: *Npy2r*$^{tm1.1(cre)Lbrl}$/RcngJ	The Jackson Laboratory	Stock No: 029285
Mouse: *Gpr65*$^{tm1.1(cre)Lbrl}$/RcngJ	The Jackson Laboratory	Stock No: 029282
Software and Algorithms		
MATLAB	MATLAB and Statistics Toolbox Release 2019b	https://www.mathworks.com/
The R Project for Statistical Computing	R Core Team, 2019	https://www.R-project.org/
Seurat v3.1.0	Butler et al., 2018	https://satijalab.org/seurat/
Enrichr	Chen et al., 2013; Kuleshov et al., 2016	https://amp.pharm.mssm.edu/Enrichr/

LEAD CONTACT AND MATERIALS AVAILABILITY

Further information and requests for resources and reagents should be directed and will be fulfilled by the Lead Contact, Stephen Liberles (Stephen_Liberles@hms.harvard.edu). Mouse lines generated in this study will be deposited at The Jackson Laboratory.

EXPERIMENTAL MODEL AND SUBJECT DETAILS

All animal husbandry and procedures were performed in compliance with institutional animal care and use committee guidelines. *Crhr2-ires-Cre* and *Gabra1-ires-Cre* mice were constructed as described below; *Gpr65-ires-Cre*, *Glp1r-ires-Cre*, *Npy2r-ires-Cre*, *P2ry1-ires-Cre* and *P2x2/P2x3*$^{-/-}$ mice were described before (Chang et al., 2015; Finger et al., 2005; Williams et al., 2016); *Vglut2-ires-Cre* and *loxP-L10-GFP* mice were gifts from Bradford Lowell (Beth Israel Deaconess Medical Center); and wild-type C57BL/6J (000664), *Calb1-ires-Cre* (028532), *Chat-ires-Cre* (006410), *Chat-GFP* (007902), *Krt8-Cre*^{ER} (017947), *Npy1r-Cre* (030544), *Piezo2-EGfp-ires-Cre* (027719), *Plcβ2*$^{-/-}$ (018064), *loxP-tdTomato* (007908), *loxP-ChR2* (012569), and *loxP-DTR* (007900) mice were purchased (Jackson Laboratory). The constitutive *GCaMP3* allele (*Rosa26-GCaMP3*) was generated by breeding *loxP-GCaMP3* (014538) with *E2a-Cre* mice (Jackson, 003314), and then crossing out the *E2a-Cre* allele. Single-cell sequencing was performed on male C57BL/6J mice; both male and female mice between 8-24 weeks old were used for all other studies, and no differences based on sex were observed.

METHOD DETAILS

Single-cell RNA sequencing

NJP ganglia were acutely harvested from 40 adult male C57BL/6J mice (across 4 technical replicates), and dissociated (75 min, 37°C, nutation, 1 mL dissociation solution per 10 mice). Dissociation solution is Dulbecco's Modified Eagle's Medium containing liberase (55 mg/ml, Roche 05401135001) and DNase (0.004%, Worthington, LS002007). Cells were pelleted (3 min, 300 g, 4°C), suspended (0.2% ovomucoid, 0.004% DNase, PBS, 200 μl), triturated with a P200 pipette tip, filtered through a 100 μm mesh cell strainer, diluted (300 μL PBS passed also through the strainer), and pelleted again (3 min, 300 g, 4°C). Cells were re-suspended (1 ml, PBS-Ca^{2+}/Mg^{2+}, which is PBS supplemented with calcium and magnesium) and loaded onto a Percoll gradient (Sigma-Aldrich, P1644) in a 14 mL round-bottom tube with three layers: 2 mL 55% Percoll in PBS-Ca^{2+}/Mg^{2+} (bottom), 2 mL 25% Percoll in PBS-Ca^{2+}/Mg^{2+} (middle) and 1 mL dissociated cells (top). After centrifugation (20 min, 800 g, 4°C), the cell-enriched fraction (~1 ml) was collected at the 25%–55% Percoll interface, diluted (4 mL PBS) and centrifuged (8 min, 800 g, 4°C). The cell pellet was re-suspended (20 μl PBS-Ca^{2+}/Mg^{2+}), and aliquots removed for cell counting and viability analysis.

Cells (10,000 per sample) were individually encapsulated in small droplets using a 10X Genomics platform (v3 chemistry). Single-cell cDNA was prepared using manufacturer's protocols, and sequenced on an Illumina NextSeq High Output platform. For analysis, fastqs from each replicate were aligned separately using Cell Ranger to a mm10 reference transcriptome that was custom modified to extend the *Glp1r* 3′ UTR. The feature-barcode matrices were loaded into Seurat (v3.1.0) for quality control, preprocessing, normalization and clustering (resolution = 1.5, PCs = 1:25) using a standard workflow that excluded cells with > 25% mitochondrial reads or < 200 unique features. Cells from the four replicates were integrated using Seurat's IntegrateData function. Sensory neurons were identified for subsequent subcluster analysis based on expression of multiple neuronal markers including *Vglut2, Prph, Tubb3, Nefl, Uchl1*, *Phox2b*, and *Prdm12*. Gene ontology enrichments were calculated using Enrichr (https://amp.pharm.mssm.edu/Enrichr/) on the ten most enriched genes in each cluster, ranked by significance (-p value) with exclusion of broadly expressed genes (pct.2 < 0.25).

Generating Cre knock-in mice

Crhr2-ires-Cre mice were generated by electroporating a vector containing an *ires-Cre* cassette and a neomycin selection cassette into 129S4/SvJae-derived J1 ES cells and selected for neomycin resistance. Appropriately targeted cells were identified by Southern blot and PCR analysis, and injected into C57BL/6 blastocysts to generate chimeric animals. The neomycin resistance gene was subsequently removed by crossing with *Act-Flpe* (Jackson, 003800). *Gabra1-ires-Cre* mice were generated by pronuclear injection of Cas9 protein, CRISPR sgRNAs targeting the *Gabra1* locus 3′ UTR, and a dsDNA vector containing an *ires-Cre* cassette with long (~4 kb) arms of homology into C57BL/6 embryos. Transgenic pups were screened by PCR analysis, and correct expression of the transgene was verified by two-color RNA *in situ* hybridization. All Cre driver lines used are viable and fertile, and abnormal phenotypes were not detected. Genotyping primers for *Crhr2-ires-Cre* mice were TTCCACAGCATCAAGCAGAC (common 5′ primer), ATGGAAAGCAAGGAGCAGAG (wt allele 3′ primer), and AGGAACTGCTTCCTTCACGA (*ires-Cre* allele 3′ primer), with differentially sized PCR products for the wild-type allele (464 bp) and knock-in allele (263 bp). Genotyping primers for *Gabra1-ires-Cre* mice were: TAACAGCGTCAGCAAAATCG (common 5′ primer), ATTCTCGGTGCAGAGGACTG (wt allele 3′ primer), and GAGGAAC TGCTTCCTTCACG (*Gabra1-ires-Cre* allele 3′ primer), with differentially sized PCR products for the wild-type allele (178 bp) and knock-in allele (375 bp).

Optogenetics

For vagus nerve optogenetics, animals were anesthetized with urethane (2 mg/g) unless otherwise specified and the left NJP superganglion was surgically exposed. An optic fiber (200 μm core, Thorlabs) coupled to a DPSS laser light source (473 nm, 150 mW, Ultralaser) was positioned for focal illumination of the vagal trunk (over the ganglion), superior laryngeal branch, petrosal branch, or the glossopharyngeal nerve respectively. Stimulation (10 s, 10-50 Hz, 5 msec pulses, 120-130 mW/mm^2) was controlled by a shutter system (Uniblitz). For epithelial cell optogenetics, *Krt8-Cre^{ER}; loxP-ChR2* mice were treated twice over three days with tamoxifen (100 μg/g in corn oil, Sigma T5648, oral gavage) ten days before testing. Animals were then anesthetized with urethane (2 mg/g), the trachea was surgically exposed, and a transverse incision was made below the ventral thyroid cartilage to expose the inferior aspect of the vocal folds. The optic fiber was positioned over the vocal folds and arytenoids, dorsal tracheal surface, or posterior oral cavity for illumination (10 s, 10 Hz, 5 msec pulses, 120-130 mW/mm^2) as described above.

Physiological measurements

Digastric muscle contraction was characterized by electromyographic recording (Biopac, EMG100C); tracheal pressure was measured by a differential pressure transducer (Harvard Apparatus, Part.No 73-0064), and was used for display of respiratory rhythms; and pharyngeal pressure was monitored by transoral insertion of a pressure transducer (Biopac TSD104A) connected to a size 3 balloon (Harvard Apparatus) coupled to an amplifier and data acquisition system (Biopac MP150). Swallows were identified by digastric muscle contraction, increases in pharyngeal pressure, transient apnea, and hyoid elevation. Subsequent quantification was performed by observing hyoid bone elevation, which was visually discernable and occurred concordantly with swallows identified through physiological measurements (Video S1). Expiratory reflexes were identified and quantified based on elevations of tracheal pressure without concurrent changes in digastric muscle EMG and pharyngeal pressure. Tongue movement and esophageal peristalsis were assessed by visual observation. Vocal fold dynamics were visualized from the inferior aspect through an incision below the cricoid cartilage using a fiber endoscope (Milliscope II, AIT) or stereomicroscope camera (Amscope).

Larynx perfusions

In animals anesthetized with urethane (2 mg/g), the trachea was surgically exposed and opened with a transverse incision 4-5 cartilaginous rings below the thyroid cartilage. A stimulus delivery port was inserted in the back of the mouth over the larynx, the distal trachea was cannulated to provide a breathing tube, and proximal trachea was cannulated to provide a stimulus exit port. Delivery and exit ports were connected to a peristaltic pump to deliver constant perfusion (0.1 ml/min) of saline or various stimuli. This slow flow rate avoids mechanical responses in nerve recordings, and the inserted oral cannula was secured with Kwik-Sil silicone adhesive (World Precision Instruments) to prevent leakage or cannula movement-induced responses. The upper airways were washed for 10 minutes, and stimuli were introduced (20 s, RT) with PBS washes between stimuli. Stimuli included water, saline (PBS: 137 mM NaCl, 2.7 mM KCl, 8 mM Na_2HPO_4, and 2 mM KH_2PO_4, pH 7.4, ~320 mOsmolar), high salt (5x PBS: 685 mM NaCl, 13.5 mM KCl, 40 mM Na_2HPO_4, and 10 mM KH_2PO_4, pH 7.4, ~1500 mOsmolar; or, for some experiments, 750 mM NaCl in water, ~1500 mOsmolar), citric acid (25 mM citric acid, pH 2.6, PBS), saccharin (30 mM, PBS), sucrose (100 mM in 2/3X PBS, ~320 mOsmolar), monosodium glutamate (100 mM in 1/3X PBS, ~320 mOsmolar), alanine (100 mM in 2/3X PBS, ~320 mOsmolar), denatonium (1 mM, PBS), quinine (1 mM, PBS), allyl isothiocyanate (3 mM, PBS) or capsaicin (16.4 μM, PBS). All perfused solutions contained Fast Green FCF (0.0025%) to track stimulus delivery. Each perfused stimulus was insulated by air to prevent mixing in the perfusion tubing; swallowing to PBS or air bubbles was never observed. Each mouse was given three stimulus trials, and the largest trial response was recorded. Trials were excluded from analysis if continuous perfusion was disrupted, for example due to mucus-induced clogging, and mice were rarely excluded if depth of urethane-induced anesthesia caused low breathing rate. For mechanical stimulation, PE-50 tubing (exit port) was advanced anteriorly toward the pharynx ten times, and the stimulation trials that evoked swallowing counted.

In situ hybridization

Single-color RNA *in situ* hybridization (ISH) was performed on cryosections (10 μm) of freshly frozen NJP ganglia as described previously (Chang et al., 2015; Montmayeur et al., 2001), and involved digoxigenin-conjugated cRNA riboprobes, alkaline phosphatase-conjugated anti-digoxigenin antibody (Roche AB_514497) and staining with NBT/BCIP (Thermo Scientific 34042). Two color ISH was performed as described previously with minor modifications. Digoxigenin-conjugated cRNA riboprobes were visualized with alkaline phosphatase-conjugated anti-digoxigenin antibody (Roche AB_514497) and Fast Red (Sigma-Aldrich F4648-50SET), while fluorescein-conjugated cRNA riboprobes were visualized with peroxidase-conjugated anti-fluorescein antibodies and TSA-Cy5.5 (Perkin-Elmer NEL766001KT). High-stringency washes used 0.2X SSC (2x20 minutes, 70°C, VWR 45001-046) and subsequent washes and antibody incubations used maleic acid buffer with 0.05% Tween-20. Phosphatase and peroxidase reporter reactions were performed according to manufacturer's protocols. Fluorescent images were analyzed with a Leica SP5 II confocal microscope, and colorimetric images were analyzed with a Nikon Ti2 Inverted microscope. cRNA probes were synthesized with fluorescein- (Roche 11685619910) or digoxigenin-conjugated (Roche 11277073910) dNTPs and transcribed *in vitro* following manufacturer's protocols (MegaScript T7 or SP6 Kits, Invitrogen AM1334 or AM1330). Probes (listed 5′ to 3′) were amplified using the following primer pairs: *Cckar* (994 bp) AGGAGGAAGATGGAAGGACC and GCTACTTATTAAGTGAGTCCC, *Gabra1* (1128 bp) TGGACAGCCCTCCCAA GATG and TCAGGCTTGACTTCTTTCGGTTC, *Crhr2* (835 bp) AAGGACCAGGGCCCAGTGCA and GGGTGGTGCAGATGCCACCC, *Mrgprd* (966 bp) AGAAGGGAGAGGCTACCAGG and GTTGGGATGCCAGAATTGGACG, *Rarres1* (772 bp) GCTGCGCTG CACTTCTTCAAC and CAGGGAGCCCAATCAGGAAAG, *Gfra3* (824 bp) ACCTCCACTGCTGATGATCCTG and ACTGCTCAGTTG CACAAGTCC, *Cpne6* (822 bp) TGGAGCAGCGAGGAAGTCAG and TTCCTGGAATGTGCTGGTGAAC, *Lamp5* (682 bp) GGACCGTTCCCAGTACAAGC and CCCTCACTTGGAACCGACAC, *Cysltr2* (930 bp) ATGGAAGTAACTGGGACCC and CTATAGAT GAACTTTGCTGAAT, *Slc17a7* (906 bp) TCCCTCGTCGCTACATCATCG and TCTGGCCTCCAATGGGTACG, *Uts2b* (553 bp) AACCTCTCTCTGGTGTGGACTC and CATTCCAGAGTGCAGCCAGTG, and *P2ry1* (1122 bp) ATGACCGAGGTGCCTTGG and TCACAAACTCGTGTCTCC.

Histology and immunochemistry

Native GFP fluorescence was analyzed in cryosections of NJP ganglia (Figures 3B, S2A, and S2B), except images in Figure 3 from *Vglut2-ires-Cre* and *Calb1-ires-Cre* mice, which involved native tdTomato fluorescence. For Figures 5A, 6D (cross-section, bottom), 6E (cross-section, bottom) 6F, 6G, 7A, S6B (cross-section), S6C, and S7A, immunohistochemistry was performed on fixed cryosections of NJP ganglia or larynx. Larynxes were obtained from mice after intracardial perfusion with cold fixative (4% paraformaldehyde, PBS) and cryopreservation (30% sucrose, PBS, 4°C, overnight) while NJP ganglia were harvested fresh and fixed *ex vivo* (4% paraformaldehyde, PBS, RT, 20 min). Tissue was sectioned (larynx: 35 μm, NJP ganglia: 12 μm), fixed (4% paraformaldehyde, PBS, RT, 10 min), washed (3xPBS), blocked (PBS, 5% donkey serum, 0.1% Triton X-100), and incubated with primary antibody diluted in blocking buffer. Antibody solutions were Chicken-anti-GFP (Abcam, AB_300798, 1:1000), Rabbit-anti-RFP (for tdTomato, Rockland, AB_2209751, 1:500), Goat-anti-HB-EGF (for DTR, R&D Systems, AF-259-NA, 1:250-1:500) or Rat-anti-KRT8/TROMA-I (The Developmental Studies Hybridoma Bank, AB_531826, 1:500). Specimens were washed (blocking buffer) and then incubated with fluorophore-conjugated secondary antibodies (PBS, 5% donkey serum). For open-book wholemount images (Figures 6D, top, 6E, top, and S6B, top) larynxes were collected fresh without fixation, cut along the ventral axis for open-book visualization, pinned flat and fixed (4% paraformaldehyde/PBS either 1 hr, RT or overnight, 4°C). Tissue was then stained for tdTomato as above, except antibody incubations (36 hours, 4°C), and subsequent washes (3x12 hours, 4°C) were longer. For visualizing alkaline phosphatase (Figures 6B and S6A), animals were perfused with PBS, and larynxes were collected, fixed (4% paraformaldehyde, 1 hr, RT), and washed in cold PBS. Tissues were then incubated (70°C, 2 hours) in alkaline phosphatase (AP) buffer (0.1 M Tris HCl pH 9.5, 0.1 M NaCl, 50 mM $MgCl_2$, 0.1% Tween20, 5 mM levamisole) and washed twice in AP buffer. AP activity was visualized with NCT/BCIP solution (ThermoFisher Scientific 34042) according to manufacturer's protocols. Stained samples were post-fixed (4% paraformaldehyde, overnight, 4°C), dehydrated through a series of ethanol washes, and cleared using a 1:2 mixture of benzyl alcohol (Sigma-Aldrich 402834-500ML): benzyl benzoate (Sigma-Aldrich B6630-1L). The tissue was then cut along the ventral axis for open-book visualization. Fluorescence was captured on Leica SP5 II and Nikon Ti2 Inverted Fluorescence microscopes; whole-mount colorimetric stainings were analyzed by light microscopy (Zeiss AxioZoom).

Calcium imaging in vagal ganglia

In vivo NJP ganglion imaging was performed as described previously (Williams et al., 2016). Briefly, *Piezo2-GCaMP** and *P2ry1-GCaMP** mice were anesthetized by isoflurane inhalation and the left ganglion was surgically exposed after severing central connections and immobilized on a stable platform for confocal imaging (Leica SP5 II) of calcium transients. Stretch of the lower airways was achieved by gas infusion of (1 l/min, 15 s) through a tracheal cannula (PE10 tubing, Braintree Scientific) inserted below the thyroid cartilage and advanced to the level of the carina. The baseline activity for each neuron was defined as the average GCaMP3 fluorescence intensity over a three-minute period preceding stimulus delivery, and cells were excluded if they failed to display maximal responses to electrical stimulation greater than seven standard deviations above their baseline means at the conclusion of the experiment. Cells were identified as responsive if (1) maximum GCaMP3 fluorescence exceeded seven standard deviations above the baseline mean, or (2) mean GCaMP3 fluorescence during the stimulation period exceeded three standard deviations above the baseline mean. Response analysis was performed blind to neuron identity.

Cell ablations and nerve transections

Targeted cell ablations were achieved by direct DT injection into NJP ganglia, as reported previously (Min et al., 2019) with minor modifications. Surgically exposed NJP superganglia were serially injected (10 × 10 nl) with DT injection solution (DT Sigma D0564, 0.05% Fast Green FCF Dye, PBS) using a Nanoject III Injector (Drummond). Different lots of DT had different minimal effective doses (0.08 to 2.0 ng), as determined in control titration experiments involving DTR immunostaining as a readout for efficiency. Animals recovered from surgery for 3-4 weeks prior to use in physiological assays. After physiological measurements, NJP ganglia were collected and the extent of ablation quantified by *in situ* hybridization and/or DTR immunofluorescent labeling. For Figure 1E, the SLN was transected bilaterally below the carotid artery before the branchpoint of the internal and external SLN branches; for Figure S3B, nerve transections were performed unilaterally or bilaterally as indicated. SLN-transected mice displayed normal vocal fold dynamics across the respiratory cycle, consistent with preservation of the RLN.

AAV-guided anatomical mapping

AAV injections into NJP ganglia were done as reported previously (Chang et al., 2015), with minor modifications. Surgically exposed NJP superganglia were serially injected (10 × 10 nl) with AAV solutions containing 0.05% Fast Green FCF Dye (Sigma) using a Nanoject III Injector (Drummond). *AAV-flex-tdTomato* was AAV9.CAG.Flex.tdTomato.WPRE.BGH (Addgene viral prep #51503-AAV9, $\sim 10^{13}$ genome copies/ml). *AAV-flex-AP* was AAV9.CAG.flex.PLAP.WPRE.BGh (custom virus, Boston Children's Hospital Viral Core, $\sim 10^{13}$ genome copies/ml). *AAV-flex-tdTomato* virus solution was diluted 1:1 with a Cre-independent *AAV-GFP* virus solution (pENN.AAV.CB7.CI.eGFP.WPRE.rBG, Addgene viral prep #105542-AAV9, $\sim 10^{13}$ genome copies/ml) prior to injection. Animals recovered from surgery and were sacrificed 4 weeks later for histology.

QUANTIFICATION AND STATISTICAL ANALYSIS

Swallows were identified by digastric muscle contraction, increases in pharyngeal pressure, transient apnea, and hyoid elevation. Subsequent quantification was performed by observing hyoid bone elevation. Expiratory reflexes were identified and quantified based on elevations of tracheal pressure without concurrent changes in digastric muscle EMG and pharyngeal pressure. During quantification of swallowing and expiratory reflexes, multiple trials (2-3) were performed per animal and since transient mucus secretion sometimes caused false negatives in individual trials, the trial with the highest number of events was used for each mouse. Respiratory minute volume was quantified by summing tidal volumes for each breath over the measurement period; custom MATLAB scripts were used to identify individual breaths by automated peak detection (at least 20% resting tidal volume) and to calculate tidal volume by integrating the area under the curve from the tracheal pressure trace. Minute volume was measured during light stimulation (ten seconds), and compared to the ten-second period preceding stimulation. Glottic area was defined based on pixel intensity, and measured in each video frame using customized MATLAB scripts. For *in vivo* ganglion imaging experiments, quantification was performed as described (Williams et al., 2016) using customized MATLAB scripts.

Data in graphs are represented as means ± SEM. All tests of statistical significance were performed using a one-sided Student's t test with R software, with the exception of analysis of Figure S4D which used a two-sided Student's t test. Expression scales for UMAP plots represent scaled and centered data from Seurat. Data points in Figures 1, 4, 5, 7C, 7D, S3A, S4B, and S4D are each derived from a different mouse; data points in Figure S5A are each derived from a different ganglion; data points in Figure S5B are each derived from different sections, with each bar representing a different mouse. Sample sizes from left to right: Figure 1D (6, 6, 6, 13, 6, 6, 6, 6, 6, 6, 6, 6), Figure 1E (8, 2, 31, 7, 13, 5, 20, 6, 17, 6), Figure 4A (2, 10, 4, 3, 8, 2, 2, 3, 2, 2, 14, 5), Figure 4B (4, 4, 4, 3, 3, 2, 2, 3, 2, 2, 8, 5), Figure 5B (9, 8, 4, 9, 9, 8, 4, 9, 9, 8, 4, 9, 9, 8, 4, 9), Figure 7C (5, 9, 5, 3), Figure 7D (17, 3, 13, 6, 20, 6, 31, 6), Figure 7E (Control: 31, 8, 7, 8, 8, 13, 8; P2x2/x3 KO: 6, 3, 3, 3, 3, 6, 3), Figure S3A (4, 3, 3, 5-6, 2, 1, 3, 2, 2, 4-5, 4-5), Figure S3B (14, 5, 5, 4), Figure S4B (4, 3, 4, 10), Figure S4D (6, 4, 6, 5, 6), Figure S5A (6, 12), Figure S5B (9, 9, 9, 7, 6, 9, 6, 11, 10, 6, 4) and Figure S7D (31, 6, 6). Calculations for latency to first swallow and interswallow interval were based on 248 swallows from 40 optogenetic stimulation trials in 4 *P2ry1-ires-Cre; loxP-ChR2* mice.

DATA AND CODE AVAILABILITY

The accession number for the single-cell transcriptome data reported in this paper is GEO:GSE145216. The accession number for other primary images and data reported in this paper is Mendeley: 10.17632/4gfm8jp6dr.1 (https://dx.doi.org/10.17632/4gfm8jp6dr.1).

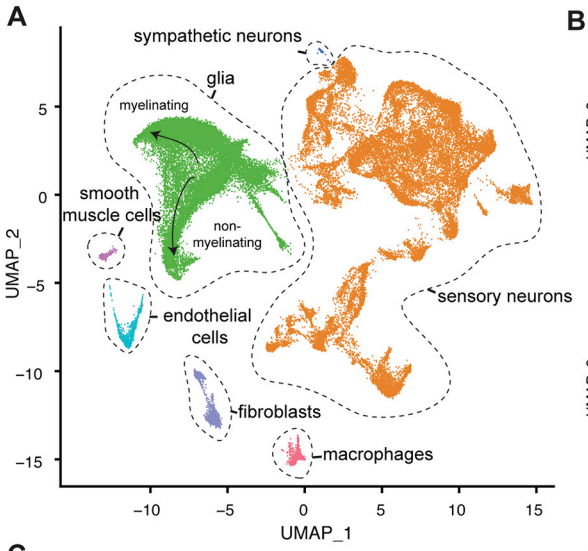

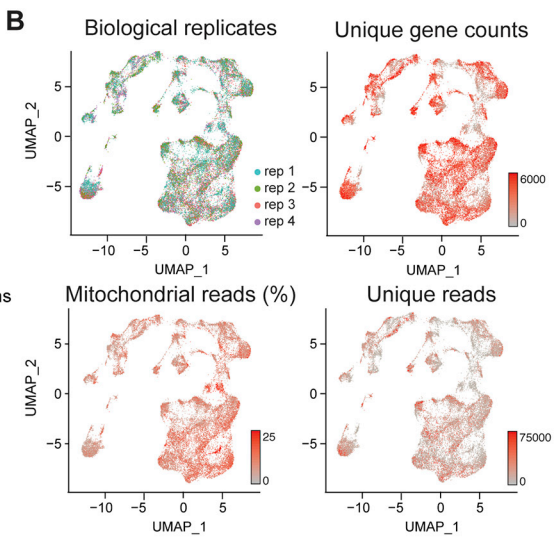

C

All cells

Total cells	46,712
Mean reads per cell	6,937
Average genes per cell	2,293

CELL TYPE	%
sensory neurons	54.46
glia	39.32
endothelial cell	1.83
fibroblast	2.23
macrophages	1.42
smooth muscle	0.62
sympathetic neurons	0.11

Sensory neurons only

Total cells	25,117
Mean reads per cell	10,816
Average genes per cell	3,135

SUBTYPE	%	SUBTYPE	%
J1	6.876	NP9	3.659
J2	3.531	NP10	3.464
J3	2.015	NP11	3.440
J4	2.011	NP12	3.360
J5	1.644	NP13	3.237
J6	1.282	NP14	3.185
J7	1.198	NP15	3.038
J8	1.147	NP16	2.664
J9	1.099	NP17	2.532
J10	0.541	NP18	2.508
NP1	6.748	NP19	2.281
NP2	4.953	NP20	1.266
NP3	4.861	NP21	1.123
NP4	4.614	NP22	1.099
NP5	4.567	NP23	1.023
NP6	4.260	NP24	0.967
NP7	3.953	NP25	0.780
NP8	3.802	NP26	0.733
		NP27	0.537

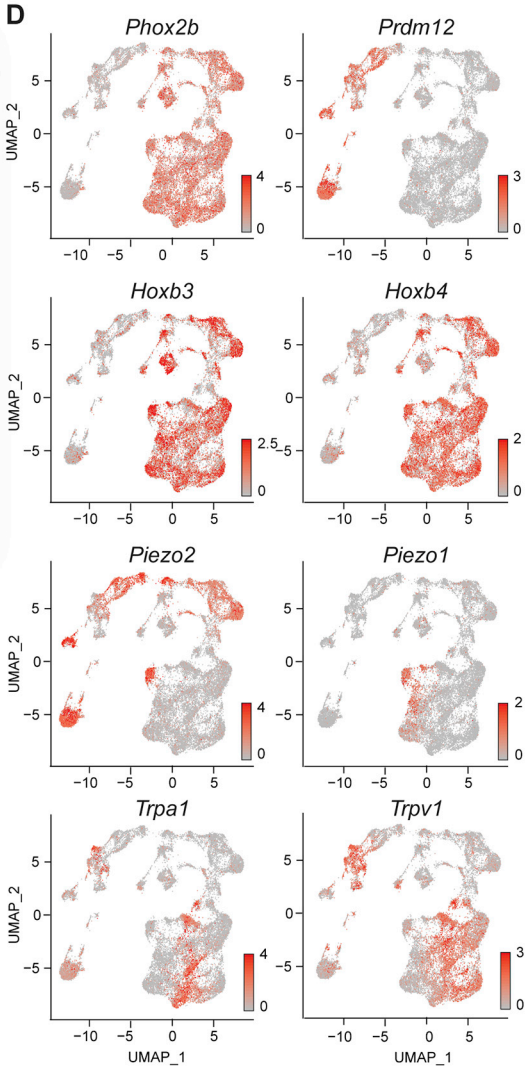

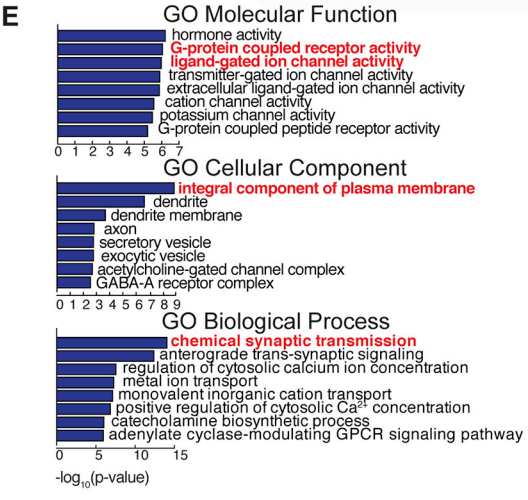

(legend on next page)

Figure S1. Single-Cell Transcriptomes of NJP Sensory Neurons, Related to Figure 2

(A) UMAP plots derived from single-cell transcriptomes indicating all cell type diversity within pooled samples (46,712 cells, 4 replicates, 10 mice per replicate). (B) UMAP plots pseudocolored by biological replicate identity, unique gene counts (nFeature_RNA), mitochondrial sequence content (%), and read counts (nCount_RNA) across sensory neuron populations. (C) Transcriptome statistics and cell type distributions across all cells (left) and sensory neurons (right). (D) UMAP plots from single-cell transcriptomes show expression of indicated genes across sensory neurons. (E) Gene ontology enrichment was calculated using Enrichr for the top 10 most differentially expressed genes from each sensory neuron cluster.

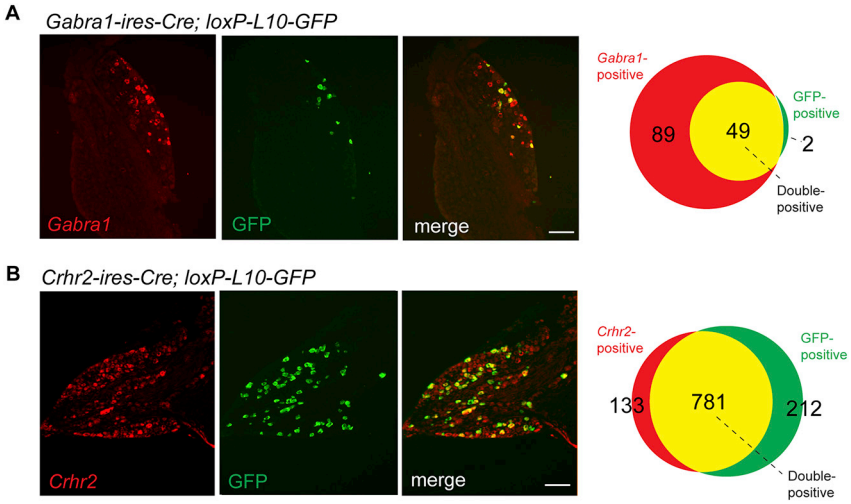

Figure S2. Validation of *Gabra1-ires-Cre* and *Crhr2-ires-Cre* Mice, Related to Figure 3

Two-color analysis in cryosections of NJP ganglia from *Gabra1-ires-Cre; loxP-L10-GFP* (A) and *Crhr2-ires-Cre; loxP-L10-GFP* mice (B). Fluorescence signal is from RNA *in situ* hybridization (red) using cRNA probes that recognize *Gabra1* (A) and *Crhr2* (B) and native GFP fluorescence (green). GFP fluorescence was imaged prior to initiation of RNA *in situ* hybridization experiments, and was superimposed *post hoc,* scale bars, 100 μm. The numbers of cells expressing the indicated mRNA alone (red), GFP alone (green) or both (yellow) were counted.

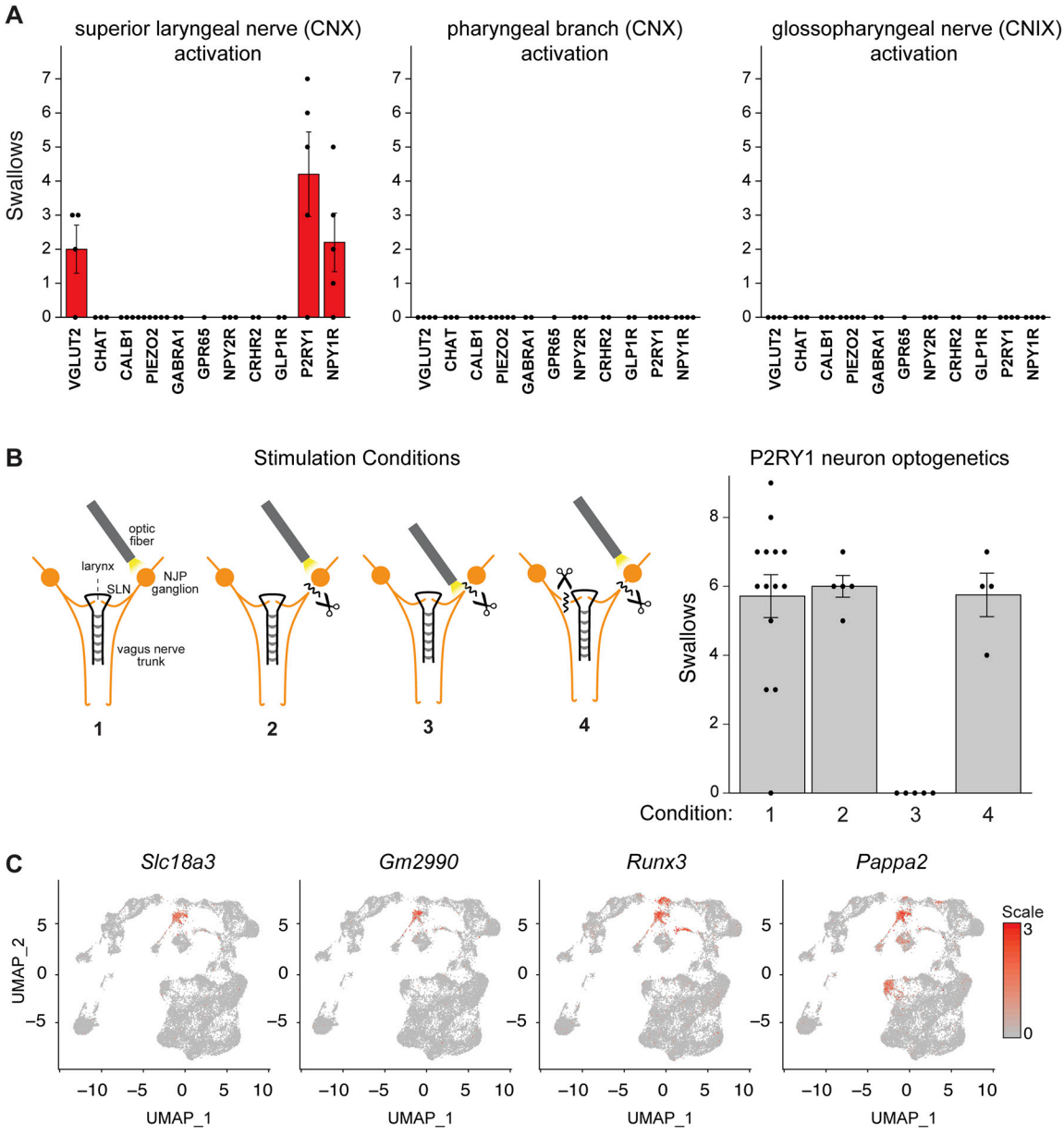

Figure S3. Nerve Branch-Specific Optogenetics, Related to Figure 4

(A) Swallows evoked by focal illumination (20 Hz) of the superior laryngeal nerve (left), pharyngeal branch of the vagus nerve (middle), and glossopharyngeal nerve (right) in *Vglut2-ires-Cre; loxP-ChR2* (VGLUT2), *Calb1-ires-Cre; loxP-ChR2* (CALB1), *Piezo2-ires-Cre; loxP-ChR2* (PIEZO2), *Gabra1-ires-Cre; loxP-ChR2* (GABRA1), *Gpr65-ires-Cre; loxP-ChR2* (GPR65), *Npy2r-ires-Cre; loxP-ChR2* (NPY2R), *Chat-ires-Cre; loxP-ChR2* (CHAT), *Crhr2-ires-Cre; loxP-ChR2* (CRHR2), *Glp1r-ires-Cre; Vglut2-ires-FlpO; RCFL-CatCh* (GLP1R), *P2ry1-ires-Cre; loxP-ChR2* (P2RY1), and *Npy1r-Cre; loxP-ChR2* (NPY1R) mice, n = 1-6 mice, mean ± SEM. (B) Swallows evoked in optogenetics experiments in *P2ry1-ires-Cre; loxP-ChR2* mice involving illumination regions and nerve transections indicated, including vagus nerve (1) trunk illumination in intact mice, (2) trunk illumination above vagus nerve transection, (3) trunk illumination below vagus nerve transection, and (4) trunk illumination above vagus nerve transection with contralateral SLN transection, n = 4-14, mean ± SEM. (C) UMAP plots from single-cell transcriptomes show expression of indicated genes.

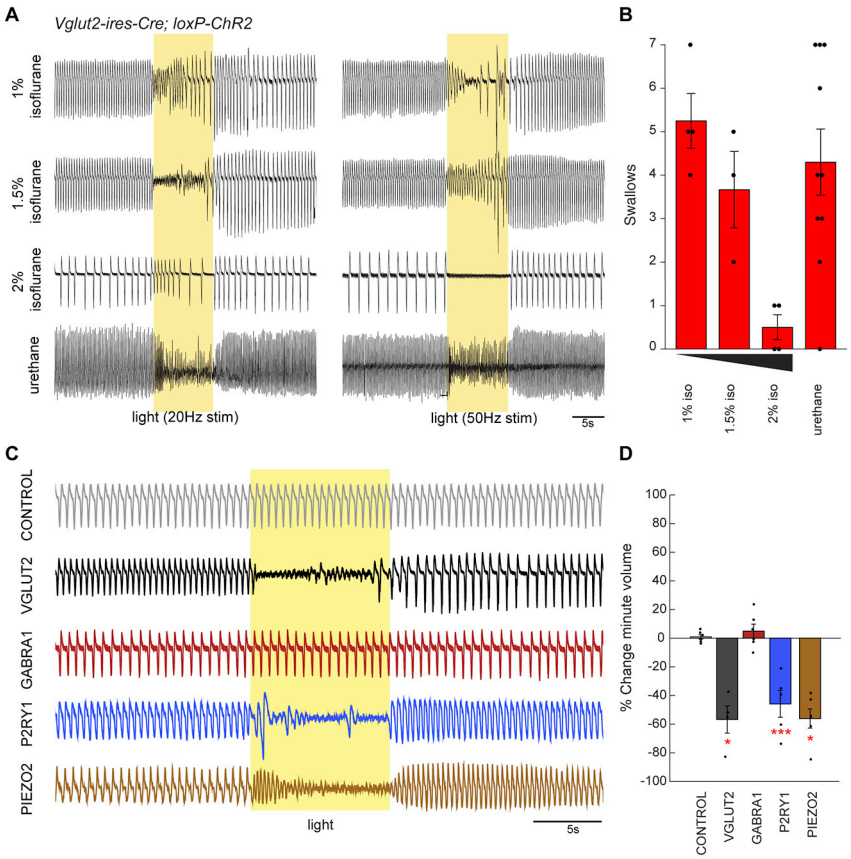

Figure S4. Anesthesia Depth Alters Optogenetically Evoked Reflexes, Related to Figure 4

(A) Representative respiratory rhythms in *Vglut2-ires-Cre; loxP-ChR2* mice were measured before, during (yellow shading) and after vagus nerve optogenetic activation (10 s, 5 msec pulses) under different anesthetics: 1%, 1.5% or 2% isoflurane (inhaled) or urethane (2 mg/g intraperitoneal injection) and frequencies (left: 20 Hz, right: 50 Hz). (B) Swallows evoked during optogenetic stimulation (20 Hz) of vagal sensory neurons in *Vglut2-ires-Cre; loxP-ChR2* mice using anesthetics indicated, n = 3–10 mice, mean ± SEM. (C) Representative respiratory rhythms (changes in tracheal pressure over time) before, during (yellow shading), and after focal illumination (20 Hz, 1.5% isoflurane) of the vagus nerve trunk in *loxP-ChR2* (CONTROL), *Vglut2-ires-Cre; loxP-ChR2* (VGLUT2), *Gabra1-ires-Cre; loxP-ChR2* (GABRA1), *P2ry1-ires-Cre; loxP-ChR2* (P2RY1), and *Piezo2-ires-Cre; loxP-ChR2* (PIEZO2) mice. (D) Quantification of respiratory minute volume changes induced by optogenetic activation (10 s) of neurons indicated, compared with pre-stimulus baseline (10 s), n = 4–6, mean ± SEM, *$p < 0.01$, ***$p < 0.0005$.

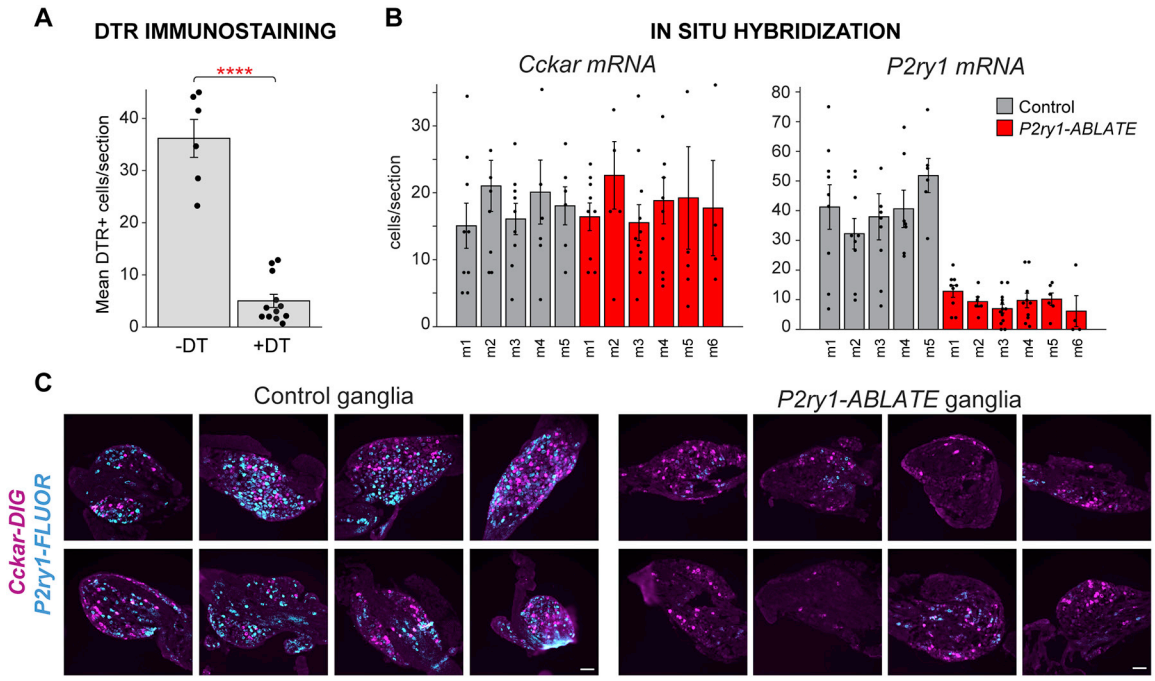

Figure S5. Validating Cell-Specific Ablation, Related to Figure 5

(A) Number of DTR-positive neurons counted following DTR immunohistochemistry in cryosections of NJP ganglia from *P2ry1-ires-Cre; loxP-DTR* mice injected with saline (-DT, n = 6 ganglia) or DT (+DT, n = 12 ganglia), mean ± SEM, ****$p < 8x10^{-5}$. (B) Two-color fluorescence *in situ* hybridization using cRNA probes to *P2ry1* and *Cckar* in cryosections of NJP ganglia from *P2ry1-ires-Cre; loxP-DTR* mice injected intraganglionically with saline (control, gray, n = 5 ganglia), or DT (red, *P2ry1-ABLATE*, n = 6 ganglia). Each bar indicates labeled cells from a single mouse, with each dot indicating cell counts from one section, mean ± SEM. (C) Representative images from cryosections of NJP ganglia from control and *P2ry1-ABLATE* mice after two-color fluorescence *in situ* hybridization using cRNA probes to *P2ry1* (cyan) and *Cckar* (magenta), scale bars: 100 μm.

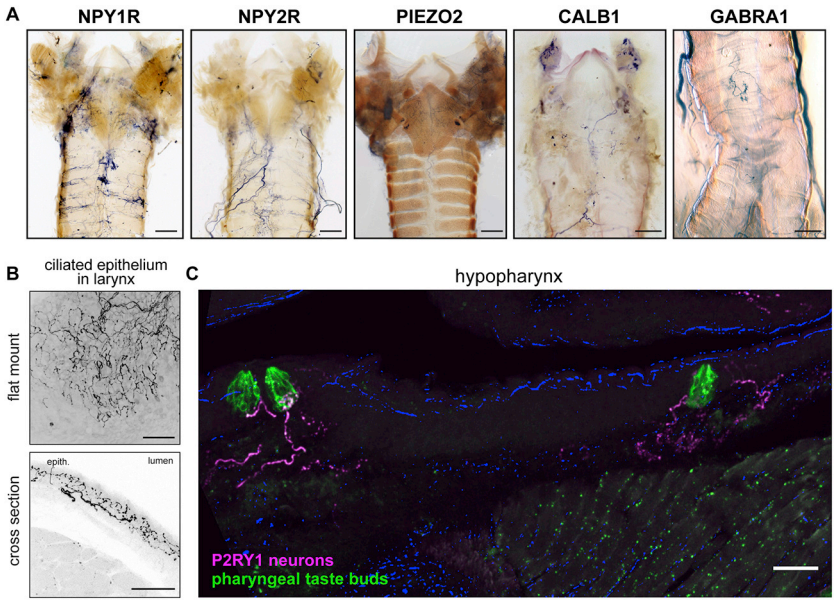

Figure S6. Diversity of Upper Airway Afferent Terminal Morphology, Related to Figure 6

(A) Neuron terminals were visualized in an open-book preparation of the larynx using an alkaline phosphatase substrate after injection of *AAV-flex-AP* into NJP ganglia of *Npy1r-Cre* (NPY1R), *Npy2r-ires-Cre* (NPY2R), *Piezo2-ires-Cre* (PIEZO2), *Calb1-ires-Cre* (CALB1) and *Gabra1-ires-Cre* (GABRA1) mice, scale bars, 500 μm. (B) Terminals in ciliated epithelium of the larynx observed following immunohistochemistry for tdTomato after injecting *AAV-flex-tdTomato* virus into NJP ganglia of *P2ry1-ires-Cre* mice, scale bars: 50 μm. (C) Two-color immunohistochemistry for KRT8 (green) and tdTomato (magenta) in cryosections of oropharynx from *P2ry1-ires-Cre* mice injected with *AAV-flex-tdTomato* in NJP ganglia, scale bar: 50 μm.

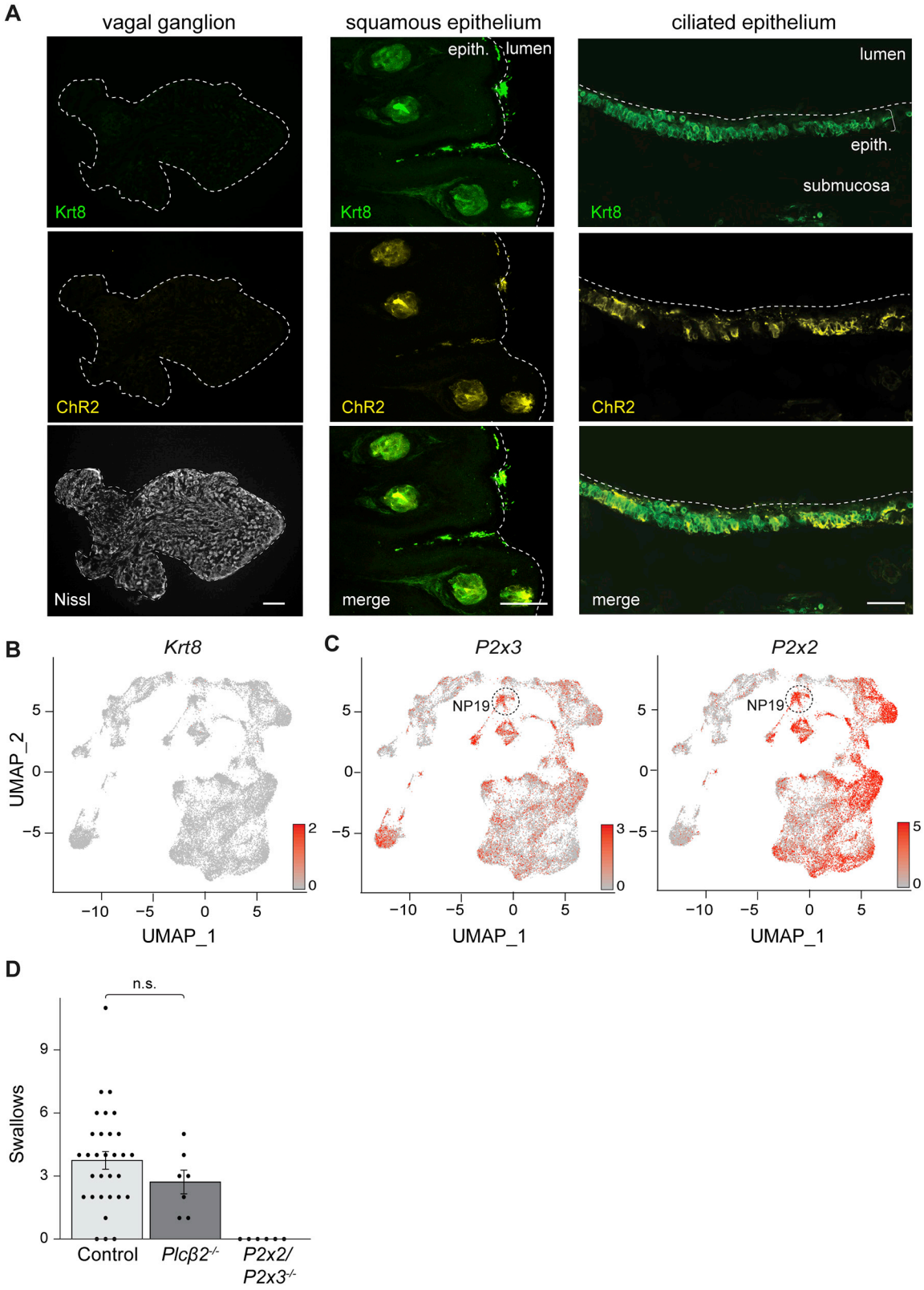

(legend on next page)

Figure S7. Expression of ChR2 in *Krt8-Cre^{ER}; loxP-ChR2* Mice; NP19 Neurons Express Ionotropic ATP Receptors, Related to Figure 7

(A) Two-color immunohistochemistry for KRT8 (green) and eYFP (yellow) in cryosections of vagal ganglia (left), laryngeal squamous epithelium (middle), and laryngeal ciliated epithelium (right) from tamoxifen-injected *Krt8-Cre^{ER}; loxP-ChR2* mice which express a ChR2-YFP fusion protein, scale bars: 100 μm (vagal ganglia) and 50 μm (epithelia). (B, C) UMAP plots showing expression of *Krt8, P2x2,* or *P2x3* in vagal sensory neurons; NP19 neurons are circled. (D) Swallows to laryngeal water perfusion (20 s) in mice indicated, n = 6-31, mean ± SEM, n.s. not significant, $p > 0.05$.